

# Chapter 5

# Fluorescence Correlation Spectroscopy (FCS)

**Radek Machán<sup>1,2</sup> and Martin Hof<sup>1</sup>**

<sup>1</sup> J. Heyrovský Institute of Physical Chemistry of ASCR, Prague, Czech Republic

<sup>2</sup> Department of Biological Sciences and Centre for Bioluminescence Sciences,  
National University of Singapore, Singapore

Contact details of corresponding author: Martin Hof, [martin.hof@jh-inst.cas.cz](mailto:martin.hof@jh-inst.cas.cz)

## Index

1. Principle and Theory.....	3
2. Instrumentation.....	4
3. Sample Preparation.....	5
4. Data Acquisition.....	6
5. Data Analysis.....	7
Calibration of the Detection Volume .....	8
Models for Fitting of Autocorrelation Curves.....	9
Choice of an Appropriate Model of Autocorrelation function .....	10
6. Artefacts in FCS.....	11
7. Technique Overview .....	13
Applications and Limitations of FCS .....	13
Selected References .....	13
8. Conclusion.....	13
References and Further Reading .....	15
Appendix.....	17
FCS with SymPhoTime 64.....	17
Test Mode .....	17
Measurement Mode.....	17
Analysis Mode.....	17

## 1. Principle and Theory

FCS is a technique which utilizes statistical analysis of fluctuations in fluorescence intensity to extract information on equilibrium processes in the sample (such as molecular diffusion or reversible chemical reactions), which are the cause of the intensity fluctuations. Low concentrations of fluorescent particles (fluorophores, fluorescently labelled molecules or supramolecular complexes) and small effective detection volumes ( $1 \mu\text{m}^3$  or smaller, typically defined by the point spread function of a confocal laser scanning microscope – CLSM) are used in FCS to obtain pronounced fluorescence intensity fluctuations<sup>[1-3]</sup>. For that reason, FCS is sometimes considered a single-molecule technique.

In an FCS measurement, time-trace of fluorescence intensity  $I(t)$  originating from the small effective detection volume  $V_0$  is recorded and its autocorrelation function  $G(\tau)$ , defined by equation (1), is calculated (pointed brackets represent averaging over all values of time  $t$ ). The shape of the autocorrelation function reflects the time-scales of the fluorescence intensity fluctuations.

$$G(\tau) = \frac{\langle I(t)I(t+\tau) \rangle}{\langle I(t) \rangle^2} \quad (1)$$

$G(\tau)$  rises steeply to its maximum value on nanosecond time-scale; the effect (called photon antibunching) is caused by a non-zero delay between two consecutive photons emitted by a single fluorophore and is related to the fluorescence lifetime and number of individual fluorescence emitters within the detection volume<sup>[4],[5]</sup>. The rise of  $G(\tau)$  is below temporal resolution of typical FCS experiments which capture only the subsequent decay of autocorrelation. Fluorescence intensity fluctuations caused by fast photophysical and photochemical processes (such as intersystem crossing to non-fluorescent triplet states or excited-state reactions) and by rotational diffusion of molecules (in the case of polarized detection) dominate the decay of  $G(\tau)$  on microsecond and sub-microsecond time-scale<sup>[6],[7]</sup>. Decay on longer time-scales is related to translational diffusion or flow of molecules in and out of the detection volume. If several processes in the sample are happening on similar time-scales, their contributions to  $G(\tau)$  are difficult to distinguish.

Theoretical models have been developed, which describe the relation between characteristics of the processes underlying fluorescence fluctuations (such as kinetic constants in the case of chemical reactions or diffusion coefficients in the case of diffusion) and the shape of the autocorrelation function calculated according to (1). Fitting  $G(\tau)$  with an ap-

propriate model yields information on equilibrium dynamics in the sample.

Investigation of diffusion of molecules and supramolecular complexes belongs among the most common applications of FCS and is, therefore, dealt with in most detail in the following text. The principle of FCS is schematically illustrated in Figure 1. Diffusion or flow causes fluctuations in the number of fluorescent particles present in the effective detection volume resulting in fluctuations in detected fluorescence intensity. Let us consider a value  $\tau_1$  of the lag time in formula (1), which is small with respect to the average residence time  $\tau_D$  of a fluorescent particle within the effective detection volume. The number of particles  $N$  present within the effective detection volume is not likely to change significantly within a time interval of the length  $\tau_1$ ;  $I(t)$  and  $I(t + \tau_1)$  are, therefore, most likely very similar to each other and the autocorrelation  $G(\tau_1)$  is close to its maximal value. The situation is analogous for other sources of fluorescence intensity fluctuations. When the fluctuations are caused by reversible transitions of the fluorophore to a dark state, the number of fluorophores in their bright state is not likely to change significantly within a lag time short with respect to the reciprocal value of the transition rate constant.

The autocorrelation function reaches its maximum at  $\tau = 0$  (disregarding the initial increase in autocorrelation caused by photon antibunching, which is below the temporal resolution of typical FCS experiments). If we consider only fluctuations caused by movement of fluorescent particles, the amplitude  $G(0)$  is inversely proportional to the average number of fluorescent particles within the detection volume<sup>[8]</sup>. FCS, apart from providing kinetic information (diffusion coefficients, kinetic constants), provides also independent estimate of concentration of fluorescent particles in the sample. Note that by the term fluorescent particle, we describe any fluorescent molecule, aggregate or complex containing at least one fluorophore which is moving as a single entity and is entering and exiting the effective detection volume at once. In the case of very large molecules (larger than the dimensions of  $V_0$ ; for example large DNA chains) labelled at multiple sites, individual segments of the molecule can behave like independent fluorescent particles and enter and exit effective detection volume at different instants<sup>[9]</sup>.

When we consider a value of lag time  $\tau_2$ , which is long with respect to  $\tau_D$ , the particle numbers  $N(t)$  and  $N(t + \tau_2)$  and, therefore, also the fluorescence intensities  $I(t)$  and  $I(t + \tau_2)$  are no more correlated and the autocorrelation  $G(\tau_2)$  is close to zero – its asymptotic value  $G(\infty)$ . The average residence time  $\tau_D$  of a fluorescent particle in the detection volume corresponds (in common models) to the lag time at which  $G(\tau)$  decays to the half of its maximal value.

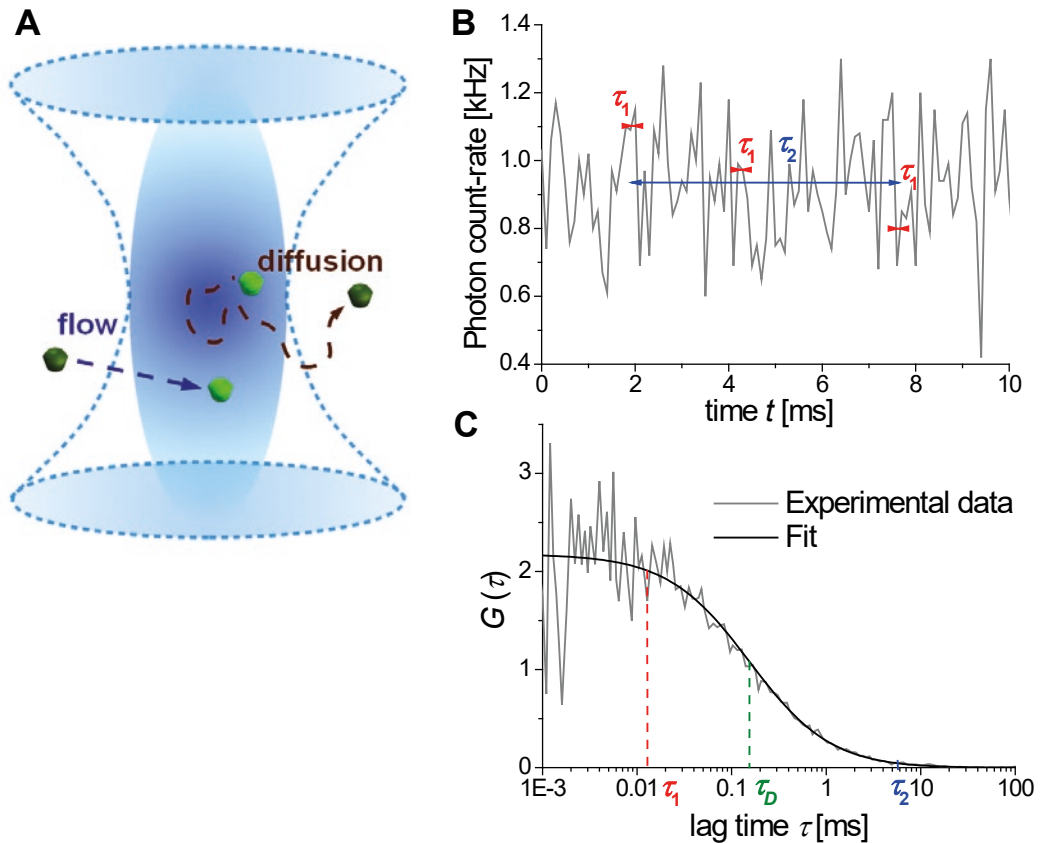


**Figure 1** Illustration of the principle of FCS. Fluorescence intensity is collected from a small effective detection volume (usually the point spread function of a confocal laser scanning microscope) (A). Recorded fluorescence intensity exhibits fluctuations (B) caused by movement of fluorescent particles out and into the detection volume (by diffusion or flow) or by reversible chemical reactions of the fluorophore. Autocorrelation function  $G(\tau)$  reflects the time-scale of the fluctuations; average residence time  $\tau_D$  of a fluorescent particle in the effective detection volume can be found by analysis of the decay of  $G(\tau)$ .

$\tau_D$  and particle number  $N$  are found by analysis of the experimentally obtained autocorrelation function. If the volume  $V_0$  is known,  $\tau_D$  and  $N$  can be used to calculate diffusion coefficient  $D$  and concentration of the fluorescent particles  $c$ .  $V_0$  is usually determined by a calibration measurement; more details on calibration in FCS and its pitfalls can be found in the section Method.

## 2. Instrumentation

As has been said in the Introduction, a CLSM is the most common instrument for FCS. The essential features of an FCS setup comprise a small effective detection volume  $V_0$  and highly efficient detection of fluorescence intensity.

The effective detection volume is defined by diffraction limited focusing of the excitation laser beam via a high numerical aperture (usually larger than 1) objective and by spatial efficiency of collecting fluorescence emission from the sample (defined by adjustment of the confocal pinhole).  $V_0$ , thus, corresponds to the point spread function (PSF) of the microscope<sup>[2],[10]</sup>.

Photomultiplier tubes (PMTs) or single photon avalanche diodes (SPADs) are used as photo-detectors for FCS, the latter ones being preferred for their higher detection efficiency<sup>[2]</sup>.

An FCS setup can be, therefore, based on most commercially available CLSMs without a need for any extensive modifications. The only modification, which is often necessary, is the addition of more sensitive photo-detectors. CLSMs designed for performing FCS and upgrades of other types of CLSMs are commercially available.

A hardware correlator used to be a common part of FCS setups. Software calculation of autocorrelation functions is, however, preferred nowadays, because it is more versatile<sup>[2],[11]</sup>. The measured time-trace of fluorescence intensity  $I(t)$  is directly stored in the computer and used to calculate  $G(\tau)$  either during the measurement or after the end of data acquisition. Software calculation of  $G(\tau)$  from stored intensity time-trace allows  $I(t)$  to be processed by application of numerical filters (which is the principle of some advanced FCS variants described in specialized chapters) or by removing sections of  $I(t)$  during which large fluorescent aggregates resided in effective detection volume. Since autocorrelation  $G(\tau)$

depends on square of fluorescence intensity, contribution of each particle to the autocorrelation function is weighted by the square of its brightness. Large aggregates, several times brighter than the average fluorescent particle in the sample, have a significant impact on  $G(\tau)$ . A rare event such as diffusion of a single bright aggregate through the detection volume can, therefore, considerably distort the whole autocorrelation function (see Figure 2).

A 2-photon microscope is also suitable for performing FCS thanks to its small PSF (which is even smaller than in the case of a CLSM)<sup>[12],[13]</sup>. The principle of 2-photon FCS is identical to 1-photon FCS and is, therefore, not discussed separately.

Alternatively any other instrumental setup can be used, which allows selective detection of fluorescence from a sufficiently small volume element within the sample. Very promising are imaging FCS modalities in which fluorescence is collected in parallel from many effective detection volumes; those are defined in the lateral plane by pixels of an imaging detector (typically an electron multiplying charge coupled device – EMCCD) and by illumination by a

thin light sheet in the axial direction. The illumination light sheet can be created by total internal reflection (TIR)<sup>[14],[15]</sup> or by a cylindrical lens such as it is done in selective plane illumination microscopy (SPIM)<sup>[16]</sup>. Imaging FCS approaches possess the advantage of performing FCS measurements in parallel in many points in the sample, in which way a statistically significant dataset can be obtained in a single measurement. This is particularly beneficial for FCS studies of intrinsically heterogeneous samples such a living cell or even multicellular structures.

### 3. Sample Preparation

Fluorescent labelling is a crucial step in preparation of samples for FCS. It has been shown that signal to noise ratio in FCS reaches the highest values when the average number  $N$  of fluorescent particles in the effective detection volume is approximately 1. The lower the particle number  $N$  is, the longer the measurement time needed to observe statistically significant number of molecules diffusing through the

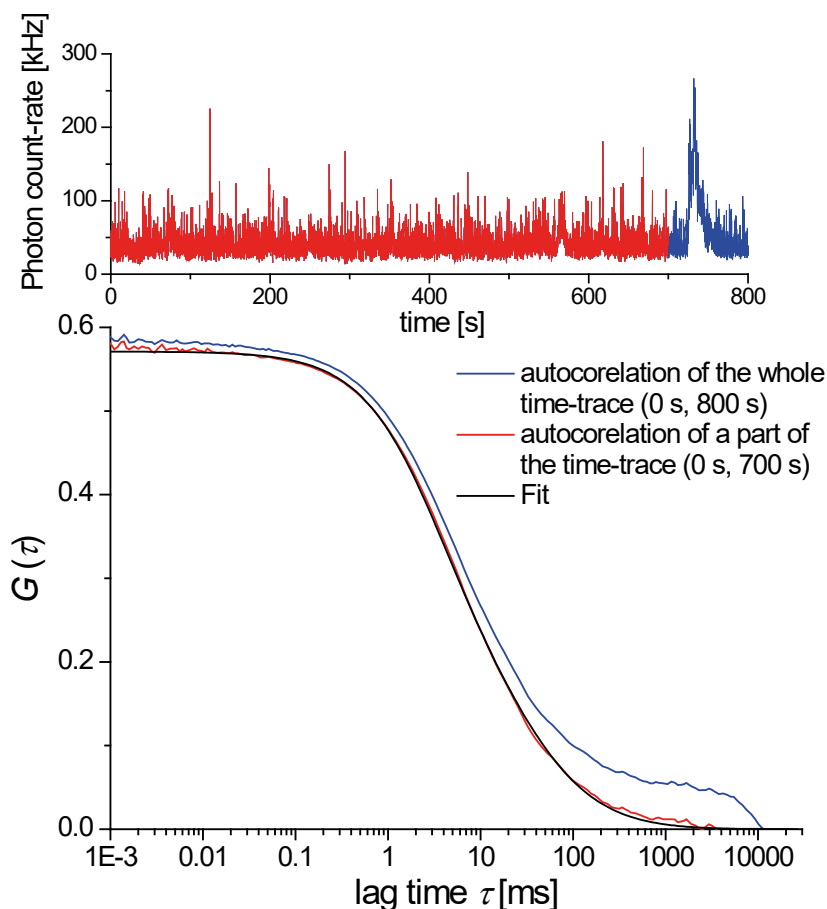


**Figure 2** Illustration of calculation of FCS autocorrelation curves. Passage of a large aggregate through the effective detection volume (manifested by a large peak in intensity time-trace – upper panel) distorts the shape of the autocorrelation function in the region of longer lag times  $\tau$ . Selecting only a part of the intensity time-trace (which is not influenced by the aggregate) results in an improvement of the shape of  $G(\tau)$ , which can be, then, fitted with model (3).

detection volume. On the other hand, high values of  $N$  result in smaller relative fluctuations and lower amplitude of autocorrelation function  $G(0)$ . Values of  $N$  in the range between 0.1 and  $10^2$  are considered well suited for FCS<sup>[3],[18]</sup>. The optimal particle numbers around 1 correspond in the case of standard confocal FCS to concentrations of fluorescent particles in nM range. Higher concentrations are used in the cases of special experimental setups with reduced effective detection volumes<sup>[19],[20]</sup>.

The choice of the fluorophore is also of considerable importance. High brightness (photon count-rate per molecule) is needed in order to acquire sufficiently high signal from each individual fluorescent particle diffusing through the detection volume. High photo-stability of the dye is also important to reduce artefacts caused by photobleaching. Photo-stability is important especially in samples where the investigated kinetics are slow and fluorophores are, therefore, undergoing excitation for prolonged periods of time. Apart from synthetic organic fluorophores, fluorescent proteins such as GFP and its mutants are frequently used in biological applications of FCS<sup>[21],[22],[23]</sup>. In this case it is crucial to find the conditions under which the fluorescent protein is expressed at concentrations suitable for FCS measurements. Quantum dots are also sometimes used for their high photo-stability<sup>[22],[24]</sup>.

Large aggregates of fluorescent particles can, due to their very high brightness, considerably distort the autocorrelation function and should be, therefore, avoided when possible. If they are present in low numbers with respect to the non-aggregated particles, the data can be cleaned from their influence, provided software correlation is used (see Figure 2).

## 4. Data Acquisition

Prior to acquiring FCS data, the instrument should be carefully aligned. FCS measurements are very sensitive to the actual shape of the effective detection volume. Proper alignment is, therefore, more critical than in the case of confocal imaging. The alignment ensures optimal photon collection efficiency through optimizing the emission light pathway of the microscope (such as mirrors and lenses directing the fluorescence emission to the detectors) in order that the maximum number of photons from the effective detection volume reaches the detector. Critical is the alignment of the confocal pinhole which has a large impact on the shape of the effective detection volume. Besides that, the correction collar of the objective needs to be adjusted to compensate correctly for the thickness and refractive index of the cover-glass.

The easiest way to optimize the pinhole position is

to measure fluorescence intensity originating from a solution of a reference fluorophore and adjust the pinhole position to reach maximal intensity at the detector. It is advisable to use higher fluorophore concentration than for FCS (for example in the  $\mu\text{M}$  range). The optimal setting of the objective correction collar can be found by searching for maximum of fluorescence intensity in a solution of a reference fluorophore, like in the case of pinhole position optimization. A more rigorous way of adjusting confocal pinhole and correction collar is via measuring FCS in a solution of a reference fluorophore and searching for the maximum of molecular brightness (total photon count-rate divided by particle number  $N$ ) of the fluorophore<sup>[25]</sup>. It is usually sufficient to perform such measurement at the end of the alignment procedure; if such a measurement is performed each time under the same experimental conditions, it serves as a good control whether the microscope is correctly aligned. Besides serving as a proof of a correct alignment of the microscope, the FCS measurement in a solution of a reference fluorophore is usually also used for calibration of the effective detection volume (discussed in more detail later).

After focusing (placing the effective detection volume) to the place of interest within the sample, fluorescence intensity  $I(t)$  is recorded. The detection volume should be ideally placed close to the centre of the CLSM field of view. Further from the centre, the dimensions and shape of the effective detection volume change due to optical aberrations. However, the deviations are relatively small within the majority of the field of view of a well-aligned CLSM (excluding the regions closest to the edges of the field of view)<sup>[26]</sup>. The acquisition time should be at least  $10^3 - 10^4$  times longer than the characteristic time-scale of the slowest investigated processes<sup>[27],[28]</sup>. When focusing into small structures (e. g. biological membranes, thickness of which is much smaller than dimensions of  $V_o$ ), long measurements may suffer from artefacts caused by movements of the structure of interest with respect to the microscope focus (e. g. membrane undulations). Such movements may result in additional apparent slow kinetics in the autocorrelation function. The optimal excitation intensity in FCS is a compromise between the requirement of high number of fluorescence photons needed for statistical accuracy of  $G(\tau)$  (a tenfold reduction of excitation intensity means approximately a hundred times longer measurement needed to reach a comparable statistical accuracy<sup>[29],[30],[31]</sup>) and the need to minimize artefacts caused by photobleaching and optical saturation (nonlinearity in the dependence of fluorescence intensity on excitation intensity resulting from depletion of the ground-state fluorophore population caused by high excitation rate). The maximal excitation intensity at which no photobleaching and saturation arte-

facts appear depends on the photophysics of the fluorophore under given conditions and on the average time it undergoes excitation (which depends on the effective detection volume dimensions and on  $D$ )<sup>[32]</sup>. For typical organic fluorophores, excitation intensities should be sufficiently lower than  $30 \text{ kW cm}^{-2}$ , a value which corresponds for usual microscope objectives to excitation powers of approximately  $100 \text{ }\mu\text{W}$  (at back aperture of the objective)<sup>[2],[30]</sup>. The excitation intensity at which optical saturation starts to play a significant role can be directly determined for each type of samples (for a particular fluorophore in a particular environment) by measuring the dependence of fluorescence intensity on the excitation intensity (a saturation curve). A linear dependence is observed at low excitation intensities; increasing deviations from linearity appear at higher intensities, until saturation is reached. Further increase of excitation intensity does not lead to any increase in the intensity of fluorescence. FCS measurements should be performed with excitation intensities corresponding to the linear region of the curve.

The influence of photobleaching and optical saturation (as well as other possible sources of artefacts in FCS such as confocal pinhole misalignment or mismatch in refractive indices between the sample and the immersion liquid on the objective) on the shape of  $G(\tau)$  have been extensively studied by the group of Enderlein<sup>[2],[30],[33]</sup>.

## 5. Data Analysis

Data analysis in FCS can be divided into two steps: the first step is the calculation of the autocorrelation function  $G(\tau)$  from the measured fluorescence intensity time-trace  $I(t)$ ; the second step is the analysis of the autocorrelation function. If a hardware correlator is used, only the second step is present, because  $G(\tau)$  represents the direct instrumental readout. If software correlation is used, only a part of the intensity time-trace  $I(t)$  can be chosen to avoid distortion of  $G(\tau)$  by large fluctuations of fluorescence intensity caused for example by the passage of a large fluorescent aggregate through the detection volume (see Figure 2).

The first step is not problematic since it follows a straightforward algorithm. Many implementation of the algorithm are readily available for the users. For example FCS software packages QuickFit (Deutsches Krebsforschungs Zentrum, Heidelberg, Germany) or FFS Data Processor (Scientific Software Technologies Center, Minsk, Belarus) can correlate data recorded by various instruments. Dedicated FCS instruments are usually supplied with software allowing correlating time-traces recorded by the respective instrument.

Let us focus in more detail on the second step, which involves more input from the user, because an appropriate model for interpretation of  $G(\tau)$  has to be chosen. Analysis of autocorrelation functions can be performed in most FCS software packages such as the above mentioned QuickFit or FFS Data Processor. Alternatively, any data processing software allowing non-linear curve fitting can be used to fit  $G(\tau)$  with a theoretical model.

The theoretical models, which describe the shape of the autocorrelation function  $G(\tau)$  are usually derived by approximating the effective detection volume by a 3-dimensional Gaussian profile (2) describing the probability  $W(R,Z)$  of detecting a photon emitted by a fluorophore located at a given position  $(R,Z)$ .  $R$  is the radial distance from the optical axis and  $Z$  is the axial coordinate ( $Z = 0$  corresponds to the focal plane);  $\omega_0$  and  $\omega_z$  are parameters describing the extent of the effective detection volume in the focal plane and along the optical axis respectively.

$$W(R,Z) = \exp\left(-2\frac{R^2}{\omega_0^2}\right) \exp\left(-2\frac{Z^2}{\omega_z^2}\right) \quad (2)$$

Some authors have derived models for more realistic shapes of effective detection volumes<sup>[10],[34]</sup>; however, the resulting models are much more complicated and not commonly used in practice. We will, therefore, mention only models derived for the 3-dimensional Gaussian approximation (2). The most basic situation is the free diffusion of a single type of particles in all 3 dimensions.  $G(\tau)$  is, in that case, described by the model (3). A detailed derivation of the model can be found in the original works on theory of FCS<sup>[8],[35]</sup>. Models applicable in other frequently encountered situations are summarized in one of the following sections.

$$G(\tau) = \frac{1}{N} \frac{1}{1+(\tau/\tau_D)} \sqrt{\frac{1}{1+(\tau/\tau_D)(\omega_0/\omega_z)^2}} \quad (3)$$

(3) can be rewritten in terms of diffusion coefficient  $D$  and concentration of fluorescent particles  $c$  (4) using their relationship to the dimensions of the effective detection volume (5) and (6) respectively<sup>[36]</sup>.

$$G(\tau) = \frac{1}{c N_A V_0} \left(1 + \frac{4D\tau}{\omega_0^2}\right)^{-1} \left(1 + \frac{4D\tau}{\omega_z^2}\right)^{-1/2} \quad (4)$$

$$\tau_D = \frac{\omega_0^2}{4D} \quad (5)$$

$$N = c N_A V_0 = c N_A \pi^2 \omega_0 \omega_z \quad (6)$$

The simple model (3) contains 3 fitting parameters:  $\tau_D$ ,  $N$  and the ratio  $\omega_z/\omega_0$  called structure parameter  $k$  and describing the shape of the effective detection volume. While  $\tau_D$  and  $N$  represent the readout parameters of the fit, structure parameter is determined by a calibration measurement and then used as a constant parameter when fitting the results of the subsequent series of measurements. Determination of the physically relevant parameters  $D$  and  $c$  requires the knowledge of  $V_0$ , which is also determined by the calibration measurement. Note, that at  $\tau = 0$ ,  $G(\tau)$  reaches its maximal value  $G(0)$ , which is inversely proportional to the number  $N$  (or concentration  $c$ ) of fluorescent particles.

### Calibration of the Detection Volume

Calibration of the detection volume is necessary for quantitative interpretation of FCS data. Calibration should be performed after any change to the experimental setup, which may affect the size and shape of the detection volume (change of excitation wavelength, of confocal pinhole, etc.); a calibration measurement is usually performed at least every day, if the identical setup is used for a longer time. There exist three approaches to the calibration in FCS<sup>[36],[37]</sup>:

1. Measurement of an FCS autocorrelation function in a solution of a reference fluorophore of exactly known concentration (or, optimally, a series of measurements with a series of concentrations);  $V_0$  is calculated from the amplitude of the autocorrelation  $G(0)$  according to (6). This calibration procedure is optimal for FCS experiments focusing on determination of concentrations via measuring  $G(0)$ , because  $V_0$  is, in this case, determined without making any assumptions concerning the shape of the effective detection volume. Deviations of the shape from the usually assumed Gaussian profile do not, therefore, affect the results. On the other hand, this calibration procedure is not sufficient for determination of diffusion coefficients, because it provides no information on  $k$  (or  $\omega_0$ ). That information can be supplemented by the second calibration procedure described below. Not all standard fluorescent dyes are suitable for concentration-based calibration; for example rhodamine 6G or some Alexa Fluor® dyes adsorb

strongly to glass surface, which causes a large uncertainty in their concentration<sup>[36]</sup>. Uncorrelated background or scattered light can lead to overestimation of  $N$  (see the section Artefacts in FCS below), which would introduce an error in  $V_0$  calibration if the fluorescence intensity is not high enough to yield the relative contribution of the parasitic signal components negligible<sup>[38]</sup>.

2. Measurement of an FCS autocorrelation function in a solution of a reference fluorophore of exactly known diffusion coefficient;  $\omega_0$  is determined from  $\tau_D$  using (5) while  $\tau_D$  is found by fitting  $G(\tau)$  with (3) or another appropriate model. Structure parameter  $k$  is also found from the fit of  $G(\tau)$  as another adjustable parameter. Increased number of free parameters naturally increases the risk of numerical instability of the fit and a good quality of autocorrelation function is important in the calibration measurement. Fortunately,  $\tau_D$  and  $k$  are not strongly correlated and the uncertainty in  $k$  affects only moderately the accuracy of  $\tau_D$  determination from the fit. The value of structure parameter for typical experimental setups ranges from 3 to 8 (depending on the magnification and numerical aperture of the objective)<sup>[37],[39]</sup> and varying  $k$  within this range has usually only minor influence on the fitted values of  $\tau_D$ .

Reference values of diffusion coefficients of standard fluorophores are for example summarized in one of the PicoQuant Application Notes<sup>[40]</sup>. Diffusion coefficient depends on temperature by Stokes-Einstein relation<sup>[40]</sup> and accurate knowledge of temperature by Stokes-Einstein relation<sup>[40]</sup> and accurate knowledge of temperature within the sample is indispensable for correct diffusion-based calibration. The reference value of diffusion coefficient must be corrected for the actual temperature in the sample for calibration purposes.

Diffusion-based calibration is optimal for FCS studies focusing on measuring diffusion coefficients, because it calibrates  $\omega_0$ , which is the crucial parameter for determination of  $D$ . However, the value of  $V_0$  calculated from  $\omega_0$  and  $k$  (6) is strongly influenced by any uncertainty in the value of  $k$  and may lead to considerable errors in the concentration determination.

3. CLSM scanning of a small fluorescent bead attached to a glass surface provides an FCS-independent determination of the dimensions and shape of the effective detection volume<sup>[37]</sup>. When a fluorescent bead of a size much smaller than the detection volume is scanned by CLSM, the resultant image shows the effective detection volume of the microscope. The accuracy of the calibration depends on the accuracy of the CLSM scanner. The image can also reveal any distortion or asymmetry of the effective detection volume, which may stem from any misalignment of

the microscope and would affect the shape of  $G(\tau)$ . The shape of the detection volume in the scan can be, however, slightly different from the effective detection during the actual FCS experiment, because the scanned bead is located directly at glass surface (at the boundary between two media of different refractive indices), while the detection volume in the actual experiment is usually located in some distance (usually between 20 to 100  $\mu\text{m}$ ) from the glass surface (unless structures located at the glass surface, like membranes adhering to glass, are investigated).

Correct calibration is crucial for absolute determination of diffusion coefficients and concentrations. However, absolute values of  $D$  and  $c$  are not essential in many FCS studies and only their relative changes are of importance. Those are fully described by relative changes in  $N$  and  $\tau_D$ , which are determined by fitting  $G(\tau)$  with the model (3) (or any other appropriate model expressed in terms of  $N$  and  $\tau_D$  – see the next section). The model contains only one parameter describing the effective detection volume – the structure parameter  $k$ . Since error in  $k$  has usually only marginal effect on  $\tau_D$ , a simplified calibration procedure is sufficient if only relative changes are investigated. The calibration usually consists of an FCS measurement (long enough to obtain good quality of autocorrelation data) in a solution of a reference fluorophore.  $G(\tau)$  is fitted with model (3) or (7) (see the next section for the model and its use) and  $k$  is determined as a free parameter. If the values of  $k$  and  $\tau_D$  obtained by the fit are in reasonable agreement with values usually obtained with the given setup and the given reference fluorophore,  $k$  can be used as a fixed parameter in fitting data from subsequent measurements and the instrument can be considered properly aligned. FCS calibration and its problems are further discussed in the section Artefacts in FCS.

### Models for Fitting of Autocorrelation Curves

Model (3) was derived for the basic situation of a 3-dimensional free diffusion of one population of particles (all having identical  $D$ ). Here we summarize other frequently used models of  $G(\tau)$ .

Photophysical processes such as transition to a dark state (such as a triplet state) are frequently apparent in  $G(\tau)$  on microsecond time-scale. To account for that phenomenon, an average fraction  $T$  of molecules in the triplet state and a characteristic time-scale  $\tau_T$  of the transition are included in the model (7)<sup>[7]</sup>.

$$G(\tau) = \left[ 1 - T + T e^{-\frac{\tau}{\tau_T}} \right] \frac{1}{N(1-T)} \frac{1}{1+(\tau/\tau_D)} \sqrt{\frac{1}{1+(\tau/\tau_D)(\omega_0/\omega_z)^2}} \quad (7)$$

Model (8) describes a more general case of a sample containing  $M$  populations of fluorescent particles; each population characterized by its diffusion time  $\tau_{Di}$ , brightness  $Q_i$ , and fraction of the particle number  $F_i$ <sup>[41]</sup>.

$$G(\tau) = \frac{\sum_{i=1}^M (Q_i)^2 F_i g_i(\tau)}{N \left( \sum_{i=1}^M Q_i F_i \right)^2} ; g_i(\tau) = \frac{1}{1+(\tau/\tau_{Di})} \sqrt{\frac{1}{1+(\tau/\tau_{Di})(\omega_0/\omega_z)^2}} \quad (8)$$

To account for transitions to triplet state, model (7) with  $T_i$  and  $\tau_{Ti}$  can be used as  $g_i(\tau)$  in (8).

Diffusion in biological systems is often far from the ideal Brownian free diffusion characterized by the simple diffusion law (9), according to which the mean square displacement of a diffusing particle within a time interval  $t$  is proportional to  $t$  (duration of the interval).

$$\langle r^2(t) \rangle = \langle (r(t) - r(0))^2 \rangle = 4Dt \quad (9)$$

Interaction of the diffusing particle with other molecules and supramolecular structures slows down the diffusion and may result in a nonlinear diffusion law, according to which the mean square displacement is proportional to  $t^\alpha$ . Such type of molecular motion is called anomalous diffusion (or anomalous subdiffusion) and  $\alpha$  ( $0 < \alpha < 1$ ) is called anomalous exponent. Anomalous exponent is present in model (10) of  $G(\tau)$  derived for anomalous diffusion<sup>[42],[43]</sup>.

$$G(\tau) = \left[ 1 - T + T e^{-\frac{\tau}{\tau_T}} \right] \frac{1}{N(1-T)} \frac{1}{1+(\tau/\tau_D)^\alpha} \sqrt{\frac{1}{1+(\tau/\tau_D)^\alpha(\omega_0/\omega_z)^2}} \quad (10)$$

If the fluorescent particles are not only moving by diffusion, but also by an oriented flow of velocity  $v$ ,  $G(\tau)$  is described by the model (11)<sup>[21]</sup>.

$$G(\tau) = \frac{1}{N} \frac{1}{1+(\tau/\tau_D)} \sqrt{\frac{1}{1+(\tau/\tau_D)(\omega_0/\omega_z)^2}} \exp\left( \left( -\frac{\tau v}{\omega_0} \right)^2 \frac{1}{1+(\tau/\tau_D)} \right) \quad (11)$$

So far we have discussed only the situation when the fluorescent particles are free to move in all three dimensions. However, in many biologically relevant samples such as biological membranes, movement of molecules is effectively restricted only to two dimen-

sions (movement along the plane of the membrane; thickness of biological membranes is several orders of magnitude smaller than the dimensions of the effective detection volume and can be, therefore, neglected). The effective detection area is, then, defined by the intersection of the detection volume of the microscope (defined by the confocal optics) and the planar structure along which molecules of interest are moving. It is, therefore, only a 2-dimensional area with Gaussian distribution of photon detection efficiency  $W(R)$ , described by the first exponential function in (2). The theoretical models of autocorrelation functions simplify considerably in the 2-dimensional case. (12) is the 2-dimensional counterpart of (3); 2-dimensional variants of other models (7, 8, 10, 11) are derived in an analogous manner<sup>[44]</sup>.

$$G(\tau) = \frac{1}{N} \frac{1}{1 + (\tau/\tau_D)} \quad (12)$$

Calibration procedure in the 2-dimensional case is apparently simpler, since there is no structure parameter  $k$  in (12). That is, however, a false impression, because calibration of effective detection volume is an important source of artefacts in FCS of planar samples (see Artefacts in FCS for further details). A slightly different definition of autocorrelation function  $G_A(\tau)$  is also frequently used.

$$G_A(\tau) = \frac{\langle I(t)I(t+\tau) \rangle}{\langle I(t) \rangle^2} \quad (13)$$

The only difference between  $G_A(\tau)$  and  $G(\tau)$  defined by (1) is in the constant offset  $G_A(\infty) = 1$ ;  $G_A(\tau)$  converges to 1, while  $G(\tau)$  to 0. The necessary modification of the theoretical models of the autocorrelation function (3, 7, 8, 10-12) is, therefore, trivial:  $G_A(\tau) = G(\tau) + 1$ . Some authors also use a factor  $\gamma$  in the amplitude of the autocorrelation function. Introduction of factor  $\gamma$  into the theoretical models only changes the definition of the effective detection volume. There is, therefore, no need to be confused by slightly different formulas of autocorrelation functions in some works.

### Choice of an Appropriate Model of Autocorrelation function

The choice of the model for fitting of  $G(\tau)$  is a crucial step in the analysis of FCS data. The general guideline is to use as simple a model as possible. Increasing the number of free parameters always improves the agreement of the model with the experimental autocorrelation curve; on the other hand,

it decreases numerical stability of the fit and increases the risk of obtaining parameter values which lack any physical meaning. The use of models with higher numbers of free parameters should be, therefore, supported either by a significant disagreement of the simpler models with the experimental curve or by an a priori knowledge of properties of the sample (for example that the sample contains a population of free fluorophore and a population of fluorophore bound to a protein or that the fluorophore is known to undergo transition to a triplet state). Statistical approaches are being developed for unbiased selection of the optimal model based on the quality of fits with individual models from a set<sup>[45]</sup>. However, those methods have not been so far implemented in any software package for FCS analysis.

When using models with large numbers of parameters, the reliability of the analysis is considerably improved by reducing the number of free parameters or introducing constraints on the range, within which the values of parameters are searched. For example the characteristic time  $\tau_T$  of transition to triplet state in model (7) is known to be around 10-3 ms for most fluorophores<sup>[7],[21]</sup>; a value of  $\tau_T$  larger than 0.1 ms is most likely an artefact of the fitting procedure.

Reduction of number of free parameters can be achieved by determining values of as many parameters as possible by additional FCS experiments and then using them as fixed parameters in the fitting procedure. Let us, for example, consider a sample containing free fluorophore and fluorophore bound to a protein. Model (8) with  $M = 2$  is appropriate in such a case. An additional measurement in a sample containing only free fluorophore yields the diffusion time  $\tau_{Df}$  (and optionally also characteristics of transition to triplet state) of the free fluorophore. The fit of the autocorrelation curve measured in the mixture of free and bound fluorophore, then, determines the remaining parameters: diffusion time  $\tau_{Dp}$  of the fluorescently labelled protein and the amplitude  $A_p$  of its contribution to the autocorrelation function; according to (8)  $A_p$  is given by (14).

$$A_p = \frac{Q_p^2 N_p}{(Q_p N_p + Q_f N_f)^2} \quad (14)$$

(14) simplifies considerably if  $Q_p = Q_f$ , which means that not more than a single fluorophore is bound to each protein and that binding changes neither its absorption cross-section nor its fluorescence quantum yield. Under such conditions, particle numbers  $N_p$  and  $N_f$  of the labelled protein and free fluorophore respectively can be determined easily from the amplitudes ( $A_p$  and  $A_f$ ) of their respective contributions to the autocorrelation function (8). If the brightness

of the free fluorophore is not equal to that of fluorescently labelled protein, more data are needed to determine particle numbers of free fluorophore and labelled protein<sup>[39]</sup>.

Constraints on the ranges within which values of free parameters are probed are of particular importance when the experimental autocorrelation function is not perfectly described by the model used for fitting. Such systematic deviations of the experimental autocorrelation function from the theoretical model are caused by instrumental artefacts (see the section Artefacts in FCS) as well as by complexity of the sample itself, which is not sufficiently described by the model. A typical problem is polydispersity of the populations of fluorescent particles, which are characterised by continuous distributions of diffusion times instead of a single  $\tau_D$  value assumed in models (3, 7, 8, 10-12). Many supramolecular structures such as micelles or vesicles always display some degree of polydispersity and macromolecules such as DNA can adopt various conformations resulting in

a distribution of diffusion coefficients. Simple models with (usually not more than 2) discrete values of  $\tau_D$  are commonly used even in such situations. If a continuous particle size distribution is present in the sample, only apparent mean values of  $\tau_D$  are extracted from the fits; if brightness of the particles depends on their size (such as in the case distribution of oligomers of various sizes), the obtained values of  $\tau_D$  tend to be biased towards the larger particles in the distribution, because the contribution to  $G(\tau)$  is weighted by the square of particle brightness (8). Maximum entropy method (MEM) fitting of  $G(\tau)$  is more appropriate when systems of polydisperse particles are studied, because MEM can perform fitting with an arbitrary continuous distribution of the parameters<sup>[46],[47]</sup>. MEM fitting is for example implemented in the FCS software QuickFit.

In general it can be concluded that the more is a priori known about the sample, the higher is the probability that the parameters obtained by fitting of  $G(\tau)$  are physically relevant (see Figure 3).

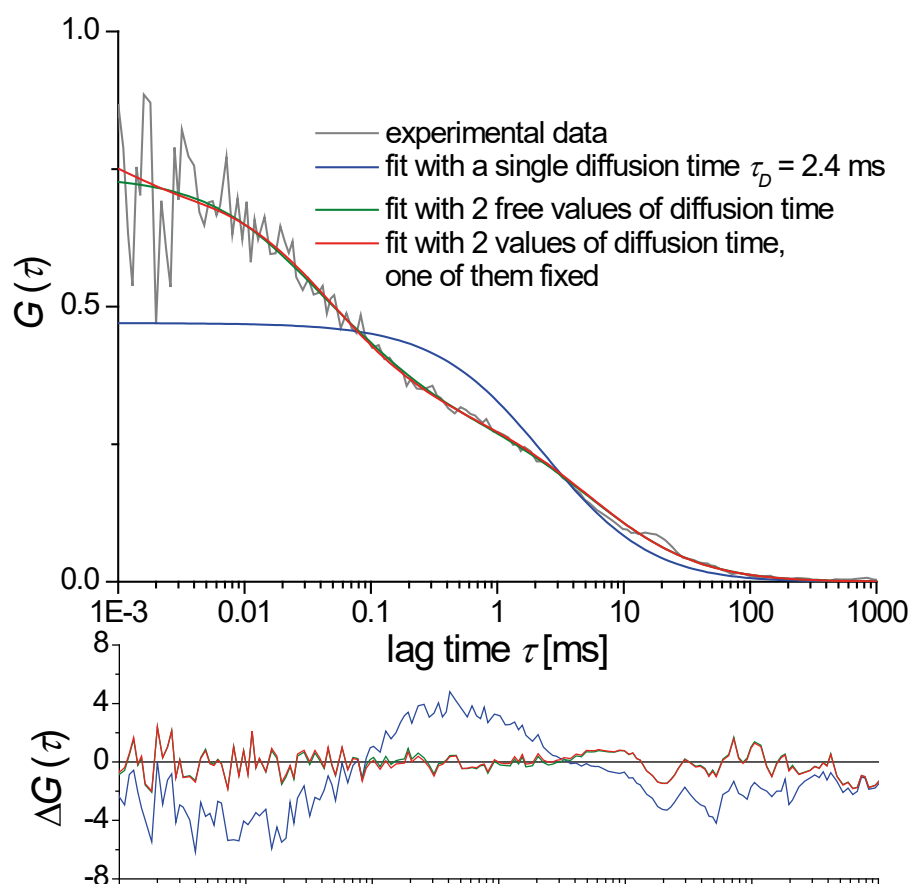


**Figure 3** Illustration of FCS fitting. The investigated sample was a suspension containing liposomes loaded with carboxyfluorescein and free carboxyfluorescein. The simple model with a single value of  $\tau_D$  (3) yields an unsatisfactory fit as can be also seen from the residues in the lower panel. A model with 2 values of diffusion time and a transition to triplet state yields a much closer fit with parameters  $\tau D1 = 6$  ms,  $A1 = 0.29$ ,  $\tau D2 = 0.076$  ms,  $A2 = 0.35$ ,  $\tau T = 0.017$  ms. A similar fit is obtained when 2 parameters are fixed using values found in an FCS measurement in a solution of pure carboxyfluorescein:  $\tau D2 = 0.048$  ms,  $\tau T = 0.001$  ms. The remaining free parameters obtained from the fit are:  $\tau D1 = 5.7$  ms,  $A1 = 0.30$ ,  $A2 = 0.42$ .

## 6. Artefacts in FCS

Like any other experimental technique, FCS can suffer from a variety of artefacts, which may introduce significant errors to FCS results and lead to their misinterpretation. The artefacts in FCS can be divided into three main categories:

1. artefacts caused by limited validity of approximations used in derivation of the theoretical models (3, 7, 8, 10-12),
2. artefacts caused by detector background and parasitic signal components and
3. artefacts related to calibration of the effective detection volume (leading to incorrect interpretation of values of  $\tau_D$  and  $N$  obtained by fitting).

Let us look at more detail on the individual types of artefacts and the ways to prevent or at least reduce their impact on the FCS data:

1. Since the theoretical models of autocorrelation function were derived assuming Gaussian profile (2) of the photon detection efficiency and monodisperse point-like fluorescent particles, the artefacts of the first type are mainly manifested in those situations where the reality deviates significantly from the above mentioned assumptions. Deviations of the actual shape of the effective detection volume from (2) can be caused for example by optical aberrations of the microscope, optical saturation or misalignment of the confocal pinhole<sup>[2],[10],[33]</sup>. Although not all of the sources can be completely avoided, it is important to take precautions to minimize the risk of artefacts where possible. A careful alignment of the confocal pinhole as well as of the correction collar of the objective are essential for FCS. The excitation intensity should be low enough to minimize distortions of the effective detection volume caused by optical saturation and photobleaching (as has been seen in the section Data acquisition).

When dimensions  $r$  of the fluorescent particles are no more negligible with respect to effective detection volume dimensions, fits of  $G(\tau)$  yield inaccurate values of  $\tau_D$  and  $N$ <sup>[48]</sup>. It has been shown that for  $r/\omega_0 > 0.2$ , both  $\tau_D$  and  $N$  are overestimated<sup>[49],[50]</sup>.

2. The influence of background and various parasitic signal components on FCS data depends on whether the parasitic counts are correlated on timescales probed by the FCS experiment. A correlated parasitic signal component influences the correlation decay  $G(\tau)$ , while an uncorrelated one only affects the amplitude  $G(0)$ . The most commonly encountered example of correlated parasitic signal components are detector afterpulses<sup>[38],[51]</sup>. Those are false counts resulting from transient effects induced in the detector by a real photon detection event. Therefore,

photon detection events and the subsequent afterpulses are correlated in time. For the commonly used detectors in FCS setups, afterpulses add to the correlation decay on  $\mu\text{s}$  and sub- $\mu\text{s}$  timescales and can be, therefore, misinterpreted as a result of fluorophore transitions to a dark state or of other fast photophysical processes. A commonly used method to prevent afterpulses from distorting the correlation functions is to split the fluorescence signal onto two detectors and then obtain  $G(\tau)$  by cross-correlating signals from the two detectors instead of auto-correlating signal from each individual detector. Since afterpulses from one detector are uncorrelated to counts from the other detector, they are not manifested in the cross-correlation function. Nevertheless the false afterpulse counts are still present in the overall signal as a non-correlated parasitic component and add to the artefacts caused by non-correlated parasitic components discussed in the following paragraph<sup>[51]</sup>.

The remaining sources of background and parasitic signal, such as detector background (thermal noise), scattered excitation photons or background fluorescence from the sample (e. g. weak fluorescence of the solvent) are typically not correlated and affect the correlation function only by lowering its amplitude  $G(0)$ , thus, leading to overestimation of the number of the fluorescent particles of interest. The effect is especially prominent in samples containing very low fluorophore concentrations. While it does not compromise the determination of  $D$ , it is a serious problem for concentration measurements by FCS. A corrected value of particle number  $N$  can be calculated from the autocorrelation amplitude  $G(0)$  using formula (15), where  $B$  denotes the average background intensity<sup>[37]</sup>.

$$N = \frac{1}{G(0)(1 + \langle B \rangle I \langle I \rangle)^2} \quad (15)$$

The correction formula (15), however, holds only when the fraction  $T$  of the fluorophores undergoing transition to a non-fluorescent state is small<sup>[37]</sup>. A more general method of eliminating both correlated and non-correlated parasitic signal components is offered by fluorescence lifetime correlation spectroscopy (FLCS)<sup>[38],[52]</sup>.

3. Calibration-related artefacts are caused by differences in effective detection volume  $V_0$  in the sample and in the reference solution. The differences are minimized by using identical experimental settings (identical temperature, identical excitation intensity, ...) during the measurement and the calibration; however they cannot be always completely avoided. Differences in refractive indices are a common cause

for different effective detection volumes. That is especially prominent in the case of intracellular FCS measurements, since cytoplasm differs significantly in refractive index from a diluted aqueous solution of a reference fluorophore<sup>[33]</sup>. Additionally, there exist some discrepancies in published values of diffusion coefficient of some standard reference fluorescent dyes<sup>[36],[53]</sup>.

An additional positioning problem exists in the case of planar samples<sup>[17],[54]</sup>. Since the excitation beam is divergent above and below its waist, placing the planar sample above or below the focal plane results in larger effective detection area and, therefore, higher values of  $\tau_D$  and  $N$ . Although uncertainties in the absolute determination of  $V_0$  do not represent a problem if only relative changes of diffusion coefficient or concentration are sought for, the positioning problem in the case of planar samples results in increased uncertainty in results of individual measurements, compromising their comparability. Therefore, several calibration-free FCS variants have been developed, which do not rely on external calibration, but contain an intrinsic measure of distance. The intrinsic calibration is typically achieved by scanning with the focus through the sample at well defined speed or with well defined steps (scanning FCS<sup>[55],[56]</sup>, Z-scan FCS<sup>[17]</sup>, ...) or by correlating intensity time-traces measured at points at well-defined distances from each other (multi-focus FCS<sup>[57],[58]</sup>, imaging FCS<sup>[59],[60]</sup>, raster image correlation spectroscopy<sup>[61]</sup>, ...).

## 7. Technique Overview

### Applications and Limitations of FCS

As has been already said in the Introduction, FCS can characterize time-scales of processes causing fluorescence intensity fluctuations as well as the concentration of independent fluorescence particles involved in those fluctuations. Movement of molecules in and out of the effective detection volume is in most cases the dominant source of fluorescence intensity fluctuations and provides information on mobility of the fluorescent particles (either diffusion coefficient or velocity of an oriented flow).

Diffusion coefficient measured by FCS can be interpreted in terms of the size of the diffusing fluorescent particles (and its changes) or in terms of viscosity and organization of the medium. The latter approach is typical for intracellular FCS measurements<sup>[43]</sup> and especially for FCS in biological membranes.

Following processes involving changes in diffusion coefficient of fluorescent particles are commonly addressed by FCS:

1. conformational changes of macromolecules; for example DNA compaction for gene therapy<sup>[9]</sup>;
2. binding of small fluorescently labelled ligands

to large molecules or supramolecular structures (such as chromatin or biological membranes). Fractions of free and bound ligand can be resolved according to (13)<sup>[62],[63],[64]</sup>;

3. aggregation phenomena and determination of critical micelle concentrations<sup>[65],[66]</sup>;
4. lateral organization of biological membranes and their artificial models<sup>[28],[67],[68]</sup>.

The second parameter provided by FCS, the concentration of fluorescent particles, is useful complementary information, which is of particular importance for investigation of aggregation phenomena. Since diffusion coefficient is approximately inversely proportional to cubic root of molecular mass (from Stokes-Einstein formula), relatively large changes in molecular mass are needed to be resolved by FCS. Oligomerization of fluorescent particles is, therefore, more reliably detected via changes in their concentration than via changes in their diffusion coefficient. The weak dependence of  $D$  on molecular mass also imposes a limitation on FCS binding studies. Association of a fluorescently labelled molecule with a binding partner of smaller or comparable molecular mass cannot be reliably resolved by FCS.

Following problems are commonly addressed by determining molecular concentrations by FCS:

1. oligomerization studies. By dividing the average photon count-rate by  $N$  determined by FCS the average brightness per particle is obtained. Comparing the obtained brightness per particle with the brightness of the monomeric fluorophore (measured ideally under identical conditions to avoid uncertainty resulting from environmental sensitivity of the fluorophore brightness) the average number of fluorophores per particle is obtained<sup>[69],[70],[71]</sup>;
2. determination of the absolute concentration of a molecules of interest within particular locations in the sample<sup>[72],[73]</sup>.

### Selected References

Theory of FCS	[8], [34], [35], [74], [76]
Artefacts and their prevention in FCS	[2], [10], [24], [30], [33], [37]
Reviews on biological or biochemical applications of FCS	[3], [18], [21], [27], [28], [36], [77], [81]
Comparison of FCS with other techniques	[82-86]

A commented bibliography on FCS can be found in the review of Thompson et al.<sup>[78]</sup>.

## 8. Conclusion

FCS analyses fluctuations of fluorescence intensity collected from a small effective detection volume (defined typically by the point spread function of a confocal microscope) and extracts information on the time-scale of processes underlying the fluctuations. Usual applications contain measurements of concentrations and diffusion coefficients of molecules or supramolecular structures moving through the detection volume or investigation of processes manifested by changes in diffusion coefficient. FCS implementation in a confocal microscope is straightforward and so is combination of FCS with confocal imaging. It is well suited for measurements in living cells and has, therefore, promising biological applications. The basic principle behind FCS is very versatile and a range of related experimental techniques is based on it (fluorescence cross-correlation spectroscopy, image correlation spectroscopy, ...). Those FCS variants have overcome some limitations of the basic FCS approach and found a variety of biological applications.

## References and Further Reading

- [1] R. Rigler, U. Mets, J. Widengren, P. Kask, *Eur Biophys J Biophys Lett*, 1993, 22, 169-175.
- [2] J. Enderlein, I. Gregor, D. Patra, T. Dertinger, U.B. Kaupp, *Chemphyschem*, 2005, 6, 2324-2336.
- [3] J. Ries, P. Schwille, *BioEssays*, 2012, 34, 361-368.
- [4] P. Kask, P. Piksarv, U. Mets, *Eur Biophys J Biophys Lett*, 1985, 12, 163-166.
- [5] J. Sýkora, K. Kaiser, I. Gregor, W. Bonigk, G. Schmalzing, J. Enderlein, *Anal Chem*, 2007, 79, 4040-4049.
- [6] P. Kask, P. Piksarv, M. Pooga, U. Mets, E. Lippmaa, *Biophys J*, 1989, 55, 213-220.
- [7] J. Widengren, U. Mets, R. Rigler, *J Phys Chem*, 1995, 99, 13368-13379.
- [8] E. Elson, D. Magde, *Biopolymers*, 1974, 13, 1-27.
- [9] N. Adjimatera, T. Kral, M. Hof, I.S. Blagbrough, *Pharm Res*, 2006, 23, 1564-1573.
- [10] S.T. Hess, W.W. Webb, *Biophys J*, 2002, 83, 2300-2317.
- [11] S. Felekyan, R. Kuhnemuth, V. Kudryavtsev, C. Sandhagen, W. Becker, C.A.M. Seidel, *Rev Sci Instrum*, 2005, 76, 083104:083101-083104:083114.
- [12] P. Schwille, U. Haupts, S. Maiti, W.W. Webb, *Biophys J*, 1999, 77, 2251-2265.
- [13] P. Schwille, K.G. Heinze, *Chemphyschem*, 2001, 2, 269-272.
- [14] B. Kannan, J.Y. Har, P. Liu, I. Maruyama, J.L. Ding, T. Wohland, *Anal Chem*, 2006, 78, 3444-3451.
- [15] N. Bag, A. Ali, V.S. Chauhan, T. Wohland, A. Mishra, *Chem Commun (Camb)*, 2013, 49, 9155-9157.
- [16] T. Wohland, X.K. Shi, J. Sankaran, E.H.K. Stelzer, *Opt Express*, 2010, 18, 10627-10641.
- [17] A. Benda, M. Beneš, V. Mareček, A. Lhotský, W.T. Hermens, M. Hof, *Langmuir*, 2003, 19, 4120-4126.
- [18] S.T. Hess, S.H. Huang, A.A. Heikal, W.W. Webb, *Biochemistry*, 2002, 41, 697-705.
- [19] H. Blom, L. Kastrup, C. Eggeling, *Curr Pharm Biotechnol*, 2006, 7, 51-66.
- [20] J. Wenger, H. Rigneault, J. Dintinger, D. Marguet, P.F. Lenne, *J Biol Phys*, 2006, 32, SN1-SN4.
- [21] P. Schwille, *Cell Biochem Biophys*, 2001, 34, 383-408.
- [22] E. Haustein, P. Schwille, *Annu Rev Biophys Biomolec Struct*, 2007, 36, 151-169.
- [23] P. Liu, S. Ahmed, T. Wohland, *Trends Endocrinol Metab*, 2008, 19, 181-190.
- [24] L.M. Davis, G.Q. Shen, *Curr Pharm Biotechnol*, 2006, 7, 287-301.
- [25] A.J. Garcia-Saez, P. Schwille, *Methods*, 2008, 46, 116-122.
- [26] X. Pan, W. Foo, W. Lim, M.H.Y. Fok, P. Liu, H. Yu, I. Maruyama, T. Wohland, *Review of Scientific Instruments*, 2007, 78, 053711.
- [27] J. Ries, P. Schwille, *Phys Chem Chem Phys*, 2008, 10, 3487-3497.
- [28] S. Chiantia, J. Ries, P. Schwille, *Biochim Biophys Acta-Biomembr*, 2009, 1788, 225-233.
- [29] Z. Petrášek, P. Schwille, *Chemphyschem*, 2008, 9, 147-158.
- [30] I. Gregor, D. Patra, J. Enderlein, *Chemphyschem*, 2005, 6, 164-170.
- [31] P. Kask, R. Gunther, P. Axhausen, *Eur Biophys J Biophys Lett*, 1997, 25, 163-169.
- [32] J. Widengren, R. Rigler, *Bioimaging*, 1996, 4, 149-157.
- [33] J. Enderlein, I. Gregor, D. Patra, J. Fitter, *Curr Pharm Biotechnol*, 2004, 5, 155-161.
- [34] H. Qian, E.L. Elson, *Appl Optics*, 1991, 30, 1185-1195.
- [35] S.R. Aragon, R. Pecora, *J Chem Phys*, 1976, 64, 1791-1803.
- [36] I.V. Perevoshchikova, E.A. Kotova, Y.N. Antonenko, *Biochemistry-Moscow*, 2011, 76, 497-516.
- [37] S. Rüttinger, V. Buschmann, B. Kramer, R. Erdmann, R. Macdonald, F. Koberling, *J Microsc*, 2008, 232, 343-352.
- [38] P. Kapusta, M. Wahl, A. Benda, M. Hof, J. Enderlein, *J Fluoresc*, 2007, 17, 43-48.
- [39] L. Yu, J.L. Ding, B. Ho, T. Wohland, *Biochim Biophys Acta-Biomembr*, 2005, 1716, 29-39.
- [40] P. Kapusta, *Absolute Diffusion Coefficients: Compilation of Reference Data for FCS Calibration*, Rev. 1, PicoQuant GmbH., Berlin, (2010), <http://www.picoquant.com/scientific/technical-and-application-notes>, Accessed: 04/05, 2014.
- [41] N.L. Thompson, in *Topics in Fluorescence Spectroscopy*, ed. J.R. Lakowicz, Plenum Press, New York 1991, Vol. 1, pp. 337-378.
- [42] D.S. Banks, C. Fradin, *Biophys J*, 2005, 89, 2960-2971.
- [43] G. Guigas, C. Kalla, M. Weiss, *Biophys J*, 2007, 93, 316-323.
- [44] R. Macháň, M. Hof, *Int J Mol Sci*, 2010, 11, 427-457.
- [45] S.M. Guo, J. He, N. Monnier, G.Y. Sun, T. Wohland, M. Bathe, *Anal Chem*, 2012, 84, 3880-3888.
- [46] P. Sengupta, K. Garai, J. Balaji, N. Periasamy, S. Maiti, *Biophys J*, 2003, 84, 1977-1984.
- [47] N. Pal, S.D. Verma, M.K. Singh, S. Sen, *Anal Chem*, 2011, 83, 7736-7744.
- [48] P. Košovan, F. Uhlík, J. Kuldová, M. Stěpánek, Z. Limpouchová, K. Procházka, A. Benda, J. Humpolíčková, M. Hof, *Collect Czech Chem*

- Commun, 2011, 76, 207-222.
- [49] K. Starchev, J.W. Zhang, J. Buffle, *J Colloid Interface Sci*, 1998, 203, 189-196.
- [50] B. Wu, Y. Chen, J.D. Muller, *Biophys J*, 2008, 94, 2800-2808.
- [51] J. Enderlein, I. Gregor, *Review of Scientific Instruments*, 2005, 76, 033102:033101–033102:033105.
- [52] P. Kapusta, R. Macháň, A. Benda, M. Hof, *Int J Mol Sci*, 2012, 13, 12890-12910.
- [53] R. Šachl, I. Mikhalyov, M. Hof, L.B.A. Johansson, *Phys Chem Chem Phys*, 2009, 11, 4335-4343.
- [54] S. Milon, R. Hovius, H. Vogel, T. Wohland, *Chem Phys*, 2003, 288, 171-186.
- [55] Q.Q. Ruan, M.A. Cheng, M. Levi, E. Gratton, W.W. Mantulin, *Biophys J*, 2004, 87, 1260-1267.
- [56] J. Ries, S. Chiantia, P. Schwille, *Biophys J*, 2009, 96, 1999-2008.
- [57] M. Burkhardt, P. Schwille, *Opt Express*, 2006, 14, 5013-5020.
- [58] T. Dertinger, V. Pacheco, I. von der Hocht, R. Hartmann, I. Gregor, J. Enderlein, *Chemphyschem*, 2007, 8, 433-443.
- [59] J. Sankaran, X.K. Shi, L.Y. Ho, E.H.K. Stelzer, T. Wohland, *Opt Express*, 2010, 18, 25468-25481.
- [60] J. Sankaran, N. Bag, R.S. Kraut, T. Wohland, *Anal Chem*, 2013, 85, 3948-3954.
- [61] M.A. Digman, C.M. Brown, P. Sengupta, P.W. Wiseman, A.R. Horwitz, E. Gratton, *Biophys J*, 2005, 89, 1317-1327.
- [62] M. Bierbaum, P.I. Bastiaens, *Biophys J*, 2013, 104, 1642-1651.
- [63] C. Caballero-George, T. Sorkalla, D. Jakobs, J. Bolanos, H. Raja, C. Shearer, E. Bermingham, H. Haberlein, *ScientificWorldJournal*, 2012, 2012, 524169.
- [64] R.H. Rose, S.J. Briddon, S.J. Hill, *Br J Pharmacol*, 2012, 165, 1789-1800.
- [65] L.L. Yu, M.Y. Tan, B. Ho, J.L. Ding, T. Wohland, *Anal Chim Acta*, 2006, 556, 216-225.
- [66] S. Nag, J. Chen, J. Irudayaraj, S. Maiti, *Biophys J*, 2010, 99, 1969-1975.
- [67] L. Wawrezynieck, H. Rigneault, D. Marguet, P.F. Lenne, *Biophys J*, 2005, 89, 4029-4042.
- [68] E. Sezgin, I. Levental, M. Grzybek, G. Schwarzmann, V. Mueller, A. Honigmann, V.N. Belov, C. Eggeling, U. Coskun, K. Simons, P. Schwille, *Biochim Biophys Acta-Biomembr*, 2012, 1818, 1777-1784.
- [69] T.A. Nguyen, P. Sarkar, J.V. Veetil, S.V. Koushik, S.S. Vogel, *PLoS One*, 2012, 7, e38209.
- [70] K. Herrick-Davis, E. Grinde, A. Cowan, J.E. Mazurkiewicz, *Mol Pharmacol*, 2013, 84, 630-642.
- [71] B. Ilien, N. Glasser, J.P. Clamme, P. Didier, E. Piemont, R. Chinnappan, S.B. Daval, J.L. Galzi, Y. Mely, *J Biol Chem*, 2009, 284, 19533-19543.
- [72] L. Erokhova, A. Horner, P. Kugler, P. Pohl, *J Biol Chem*, 2011, 286, 39926-39932.
- [73] S.R. Yu, M. Burkhardt, M. Nowak, J. Ries, Z. Petrasek, S. Scholpp, P. Schwille, M. Brand, *Nature*, 2009, 461, 533-536.
- [74] D.E. Koppel, *Phys Rev A*, 1974, 10, 1938-1945.
- [75] T. Wohland, R. Rigler, H. Vogel, *Biophys J*, 2001, 80, 2987-2999.
- [76] J. Enderlein, I. Gregor, D. Patra, J. Fitter, *J Fluoresc*, 2005, 15, 415-422.
- [77] Z. Földes-Papp, U. Demel, W. Domej, G.P. Tilz, *Exp Biol Med*, 2002, 227, 291-300.
- [78] N.L. Thompson, A.M. Lieto, N.W. Allen, *Curr Opin Struct Biol*, 2002, 12, 634-641.
- [79] A. Shahzad, G. Kohler, *Appl Spectrosc Rev*, 2011, 46, 166-173.
- [80] V. Vukojevic, A. Pramanik, T. Yakovleva, R. Rigler, L. Terenius, G. Bakalkin, *Cell Mol Life Sci*, 2005, 62, 535-550.
- [81] O. Krichevsky, G. Bonnet, *Rep Prog Phys*, 2002, 65, 251-297.
- [82] L.M. Davis, P.E. Williams, H.M. Cain, D.A. Ball, C.G. Parigger, E.D. Matayoshi, K.M. Swift, *Biophys J*, 2002, 82, 43A-43A.
- [83] Y. Chen, B.C. Lagerholm, B. Yang, K. Jacobson, *Methods*, 2006, 39, 147-153.
- [84] L. Guo, J.Y. Har, J. Sankaran, Y.M. Hong, B. Kannan, T. Wohland, *Chemphyschem*, 2008, 9, 721-728.
- [85] D.E. Koppel, D. Axelrod, J. Schlessinger, E.L. Elson, W.W. Webb, *Biophys J*, 1976, 16, 1315-1329.
- [86] D.M. Owen, D. Williamson, C. Rentero, K. Gaus, *Traffic*, 2009, 10, 962-971.

## Appendix

### FCS with SymPhoTime 64

Here we show how to perform basic FCS measurements and data analysis using the SymPhoTime 64 software (PicoQuant, Berlin, Germany). The software controls PicoQuant data acquisition cards, which record time-tagged time-resolved fluorescence data, and performs various types of analysis of those data, including calculation and fitting of FCS correlation functions. SymPhoTime 64 controls PicoQuant confocal microscopes (such as MicroTime 200); in the case of microscopes from other manufacturers upgraded with a PicoQuant data acquisition card, a dedicated microscope software is needed to control the settings of the microscope, acquire images and select a point for the FCS measurement. The subsequent recording of fluorescence intensity time-traces and their FCS analysis is performed by SymPhoTime 64. The software also controls PicoQuant pulsed laser drivers (Figure 1, 4), if it is included in the setup. Pulsed lasers are, however, needed only for time-resolved measurements are not necessary in an FCS setup.

### Test Mode

After setting a point for measurement, acquisition of fluorescence intensity time traces by SymPhoTime 64 can begin. The main window of the program has 3 main panes: Test, Measurement and Analysis (Figure 1, 1). Data acquired in the Test mode are not saved; they are only displayed in real time on the screen to aid alignment of the instrument and optimizing settings for the measurement. Three modes are available for the real time display: TCSPC, Time Trace and FCS (Figure 1, 2). The TCSPC pane displays the photon arrival histogram; since TCSPC data are not required in standard FCS, we will not discuss this display mode further. Time Trace is the most basic mode displaying the real time value of detected fluorescence intensity (Figure 1). If signal from multiple detectors is fed to the data acquisition card, a time trace for each individual detector is shown. Besides the graphic display, numerical values of average and maximum count-rate for each detection channel are shown (Figure 1, 3).

The real time intensity time trace is useful for focusing to the structure of interest (e. g. if the fluorescently labelled molecules of interest are located in the plasma membrane of a cell, by changing the axial position of the focus two maxima of fluorescence intensity can be found corresponding to the lower and to the upper membrane). Besides that, the time trace can be used to optimize the pinhole position by measuring intensity originating from a fluorophore solution (it is advisable to use in this case a higher concentration of fluorophore than for FCS).

The FCS pane in the Test mode (Figure 2) shows correlation functions calculated in real time from the detected time traces (similarly to the output from a hardware correlator). Autocorrelations of signals from individual detectors and cross-correlation between them are shown. However, in the situation shown in Figure 2 only a single detector receives fluorescence signal; the other detector contributes only its thermal noise. Maximum and average count-rate and the amplitude of the displayed correlation function are shown next to the graphic display (Figure 2, 1). The particle number corresponding to the amplitude is also shown as well as the particle brightness obtained by dividing the average count-rate by the particle number. Brightness of a reference fluorophore is a good indicator of the quality of alignment of the setup. The optimal correction ring settings can be found by searching for the maximum brightness. To aid the alignment procedure, any of the values can be displayed in a larger window (by clicking on the displayed value) (Figure 2, 2).

### Measurement Mode

After optimizing the data acquisition in the Test mode, we can switch to the Measurement pane (Figure 3 and 4), in which the recorded data are stored for subsequent analysis. Before starting the measurement, the file name for the dataset should be defined; additionally, any information on the instrument settings or on the sample details can be noted down to be saved together with the data (Figure 3, 1). The data acquisition is then started by the Start button and terminated by the Stop button (Figure 3, 2); alternatively the acquisition time can be defined and the acquisition then stops automatically after the defined time has elapsed (Figure 3, 3). The main window is divided into three panels; the upper one displays the correlation function calculated in real time, the lower left panel shows the TCSPC histogram and the bottom right panel the intensity time trace.

### Analysis Mode

After the data acquisition has finished, we proceed to the analysis of the stored data. In the Workspace explorer on the left hand side of the main program window we select the file to be analysed (Figure 5). The real time calculated correlation functions (recognised by a filename of the following structure: Name\_OFCS.pqres) are stored alongside the raw data. We are, however, not going to use this correlation function. We will, instead, calculate the correlation function again from the stored raw data. This will allow us to correct for some common FCS artefacts as mentioned in the main text. After selecting the data file, we switch to the Analysis pane in which various modes of analysis are offered. We select the FCS

menu, which offers several FCS modalities, from which we choose the basic FCS analysis (Figure 5). The window for FCS correlation calculation is shown in Figure 6. The Intensity time trace is shown in the upper panel. By sliding the red start and stop markers (Figure 6, 1) an arbitrary part of the time trace can be selected for analysis. This is useful when a part of the time trace is affected by movement of large aggregates, by bleaching etc. The range of lag-times for which the correlation is calculated can be selected (Figure 6, 2). If Lagtime Min. is set to 0, the shortest lag-time will be determined by the software based on the temporal resolution of the data. If pulsed excitation is used, FLCS can be used to correct for background and detector afterpulsing (Figure 6, 3). Explanation of the method is beyond the scope of this appendix; we will use it here, therefore, only as a “black box” feature. If continuous wave excitation is used, distortion of the correlation function caused by afterpulsing can be prevented by splitting the fluorescence emission onto two detectors and cross-correlating signals from them (see Figure 4; the cross-correlation function does not contain the steep initial decay of correlation caused by detector afterpulses). After pressing the Calculate button (Figure 6, 4), correlation function is calculated and displayed in the main panel. The correlation function can be saved (Figure 6, 5) for further analysis.

Since the sample for which we have just obtained the autocorrelation function was the solution of a calibration dye, we will use it to calibrate the effective detection volume. We select the saved autocorrelation function in the Workspace explorer and in the FCS analysis menu (Figure 5) we choose FCS calibration. That brings us to a curve fitting window (Figure 7). The default fitting model offered is that with a single diffusion time and a single dark state, which is suitable for most calibration dyes. If we know that our calibration dye has no dark state, we can switch to a simpler model by pressing the Exclude Triplet button. If we are calibrating the effective detection volume using the known value of  $D$  of our calibration dye, we fill in the reference value of  $D$  (Figure 7, 1). We can start the fitting by performing Initial Fit (Figure 7, 2), which searches over broader ranges of parameter values and is, thus, more likely to converge even if the initial parameter values are far from the optimal ones. Subsequently we can perform the Fit till self-consistency is reached (parameter values do not change, only fluctuate around their minima, during further fitting iterations). If the quality of the fit is good and the parameter values are reasonable, we can save the obtained characteristics of the effective detection volume (its volume and structure parameter  $\kappa$ ) (Figure 7, 3). Those will be then used as default values in the FCS fitting window (Figure 8). Ideally we should perform multiple calibration

measurements to check the reproducibility of the parameters.

When we afterwards measure any other dataset and calculate the correlation function (Figure 6), we can choose to proceed to fitting of the correlation function (Figure 6, 6). By default, the simplest model for pure 3-dimensional diffusion (single  $D$ , no dark state) is offered in the fitting window (Figure 8, 1). If that model does not fill well the curve (as is the case in Figure 8), we can select a more complex model, for example the model with a dark (triplet) state (Figure 9, 1). A significantly better fit is obtained as can be seen from the residuals as well as from the  $\chi^2$  value (Figure 9, 2).

Another example of autocorrelation function fit is shown in Figure 10. It is obvious that the fit is not perfect (especially in the region around 10 ms). Nevertheless, knowing the non-ideal nature of the sample (liposomes prepared by sonication, which are intrinsically polydisperse and prone to aggregation; aggregates being most likely responsible for the deviations between the fit and the experimental curve around 10 ms lag-time), we may consider the fit to be an acceptable one giving a good estimate of the typical diffusion coefficient and concentration of the liposomes. A more complex model may yield a slightly better fit; however, the parameters thus obtained may be artificial and lacking direct physical interpretation.

The curve in Figure 11 cannot be satisfactorily fitted with the model with a single  $D$  and single dark state and definitely requires a more complex model for its description. The knowledge of the nature of the sample is helpful for selecting which model to use. Knowing that the sample contained a mixture of free dye and of fluorescently labelled liposomes, a model with two values of  $D$  (Figure 12, 1) and a single dark state is expected to describe the experimental data. That is indeed the case as shown in Figure 12. The individual values of  $D$  retrieved from the fit agree within the margin of error with the values obtained from measurements in samples containing only one of the components (free dye in Figure 7 and liposomes in Figure 10). This is, however, not always the case. Keeping at least one of the diffusion times fixed to a value obtained separately in a sample containing only one of the components significantly improves reliability of fitting with two diffusion times.

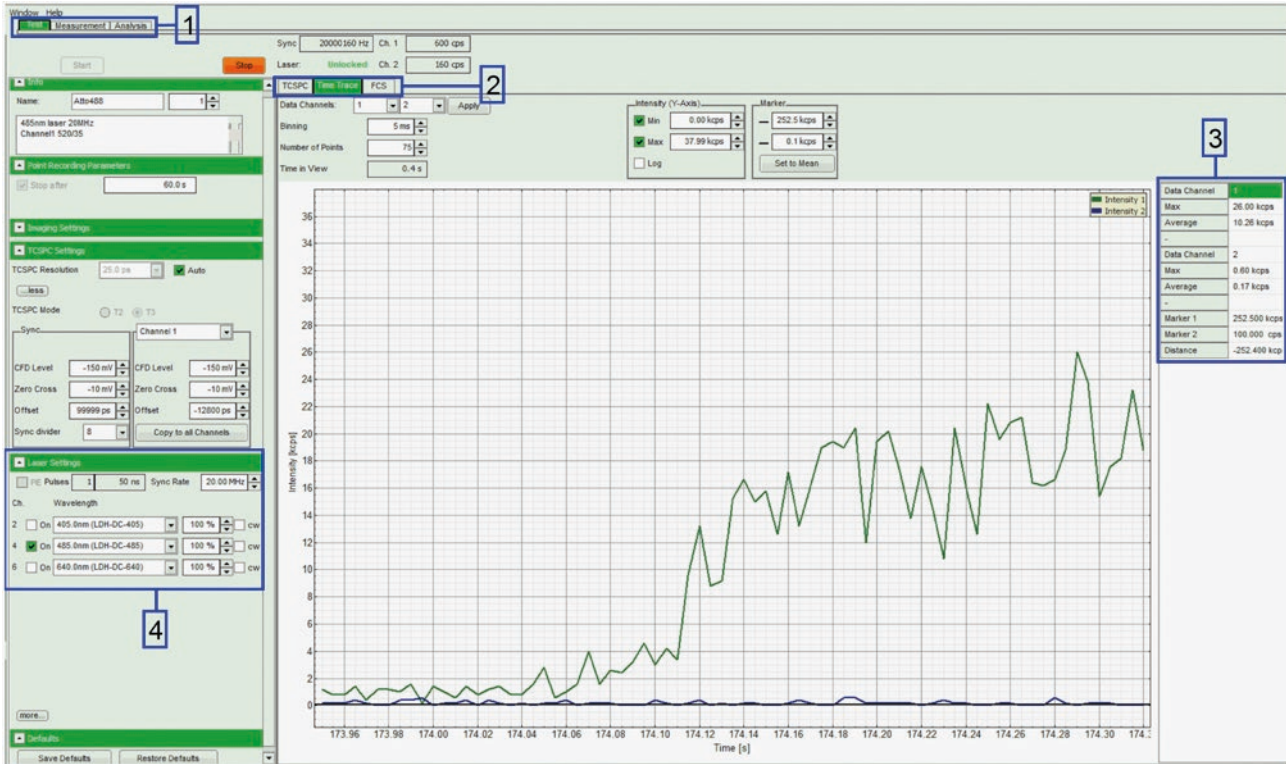


Figure 1

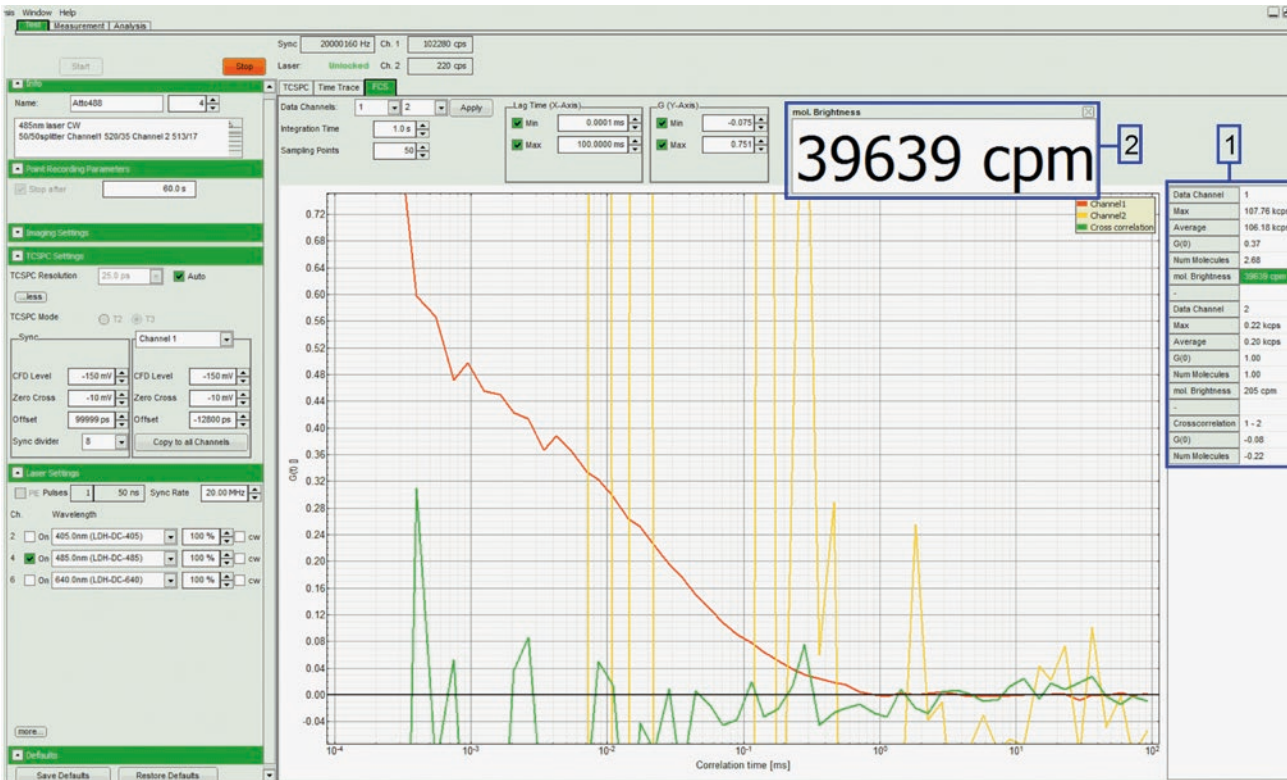


Figure 2

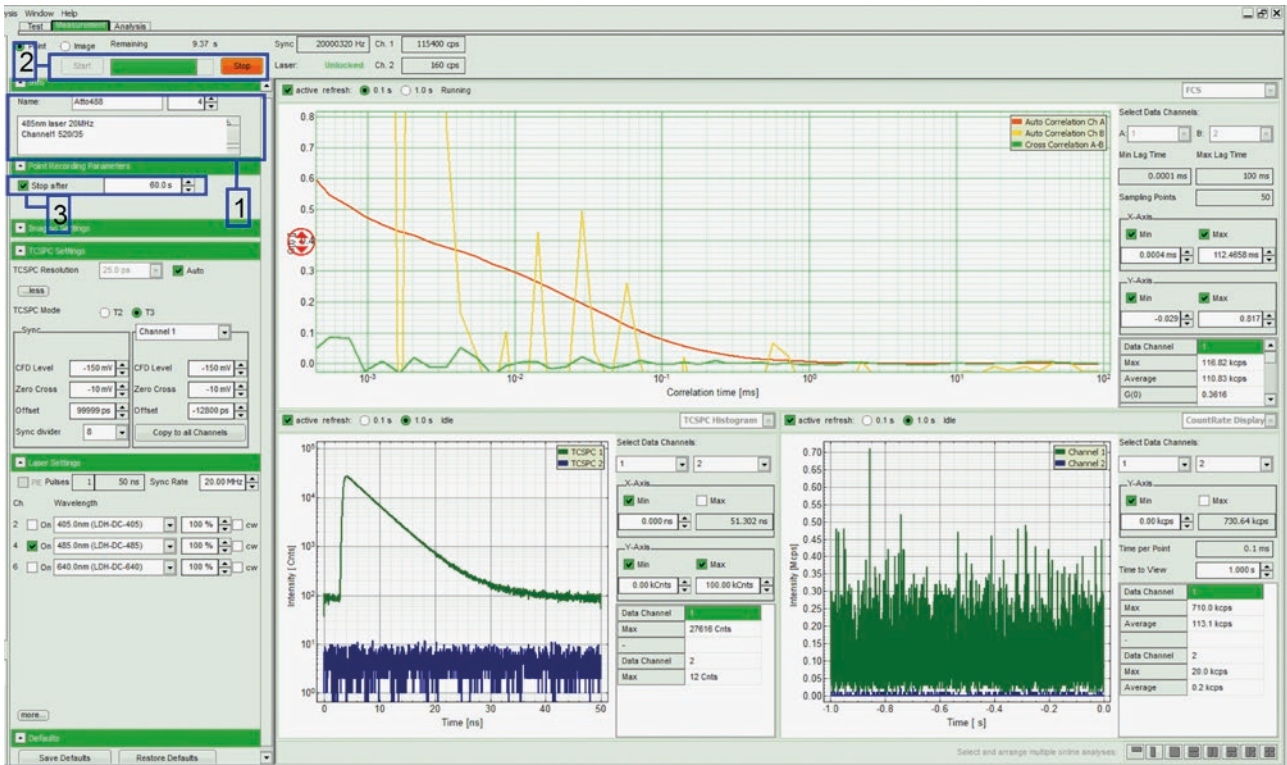


Figure 3

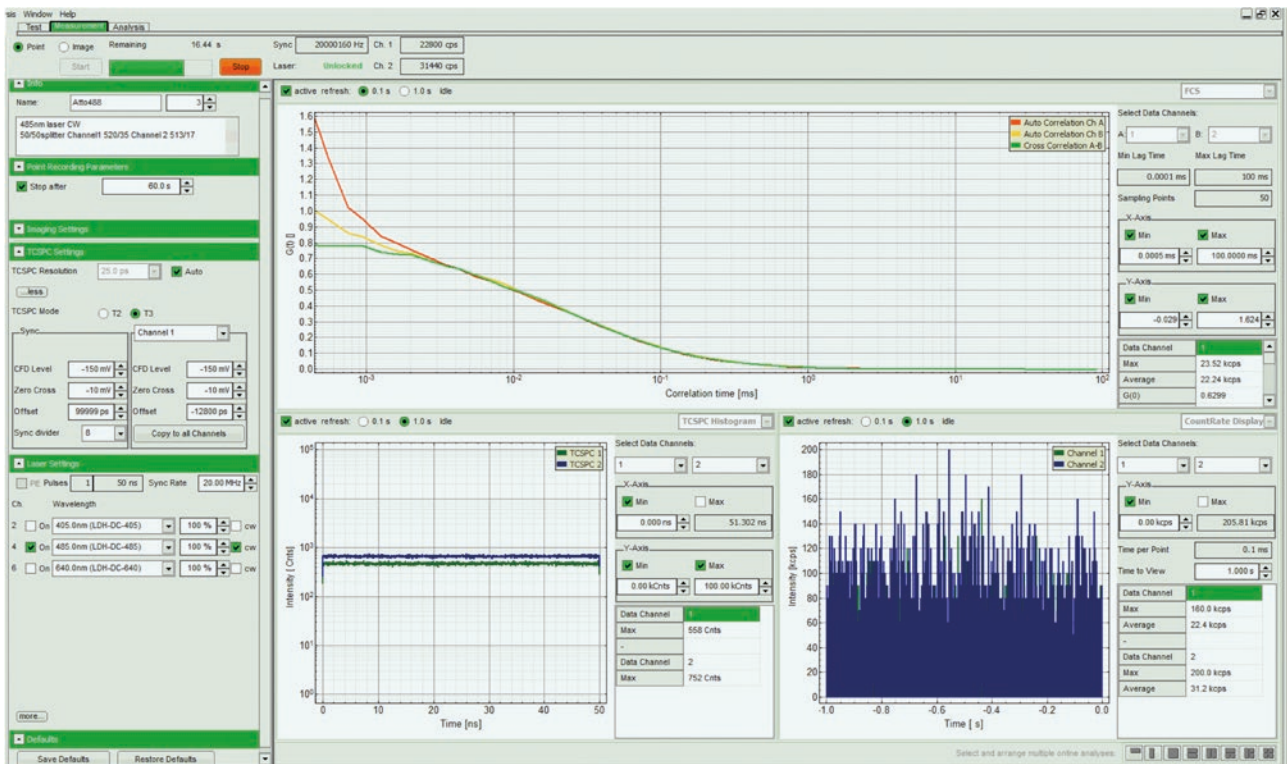


Figure 4

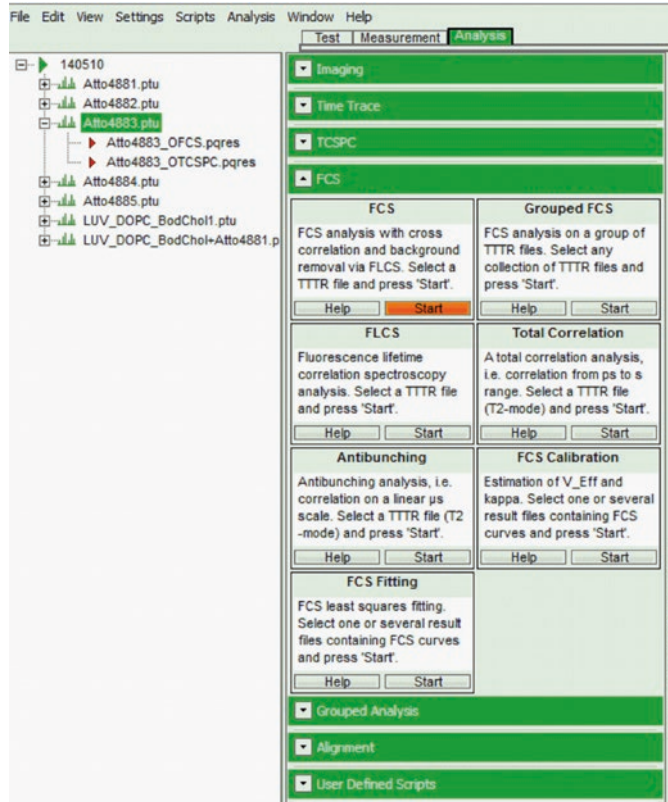


Figure 5

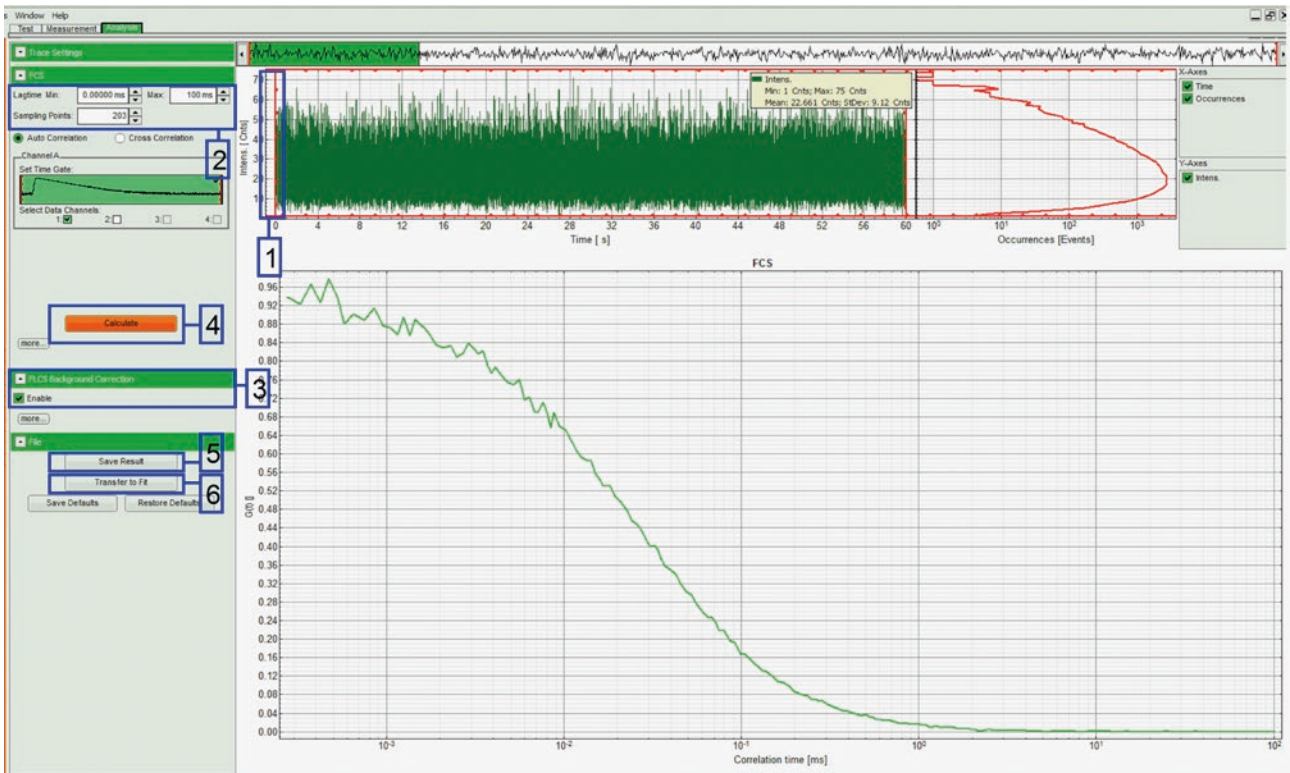


Figure 6

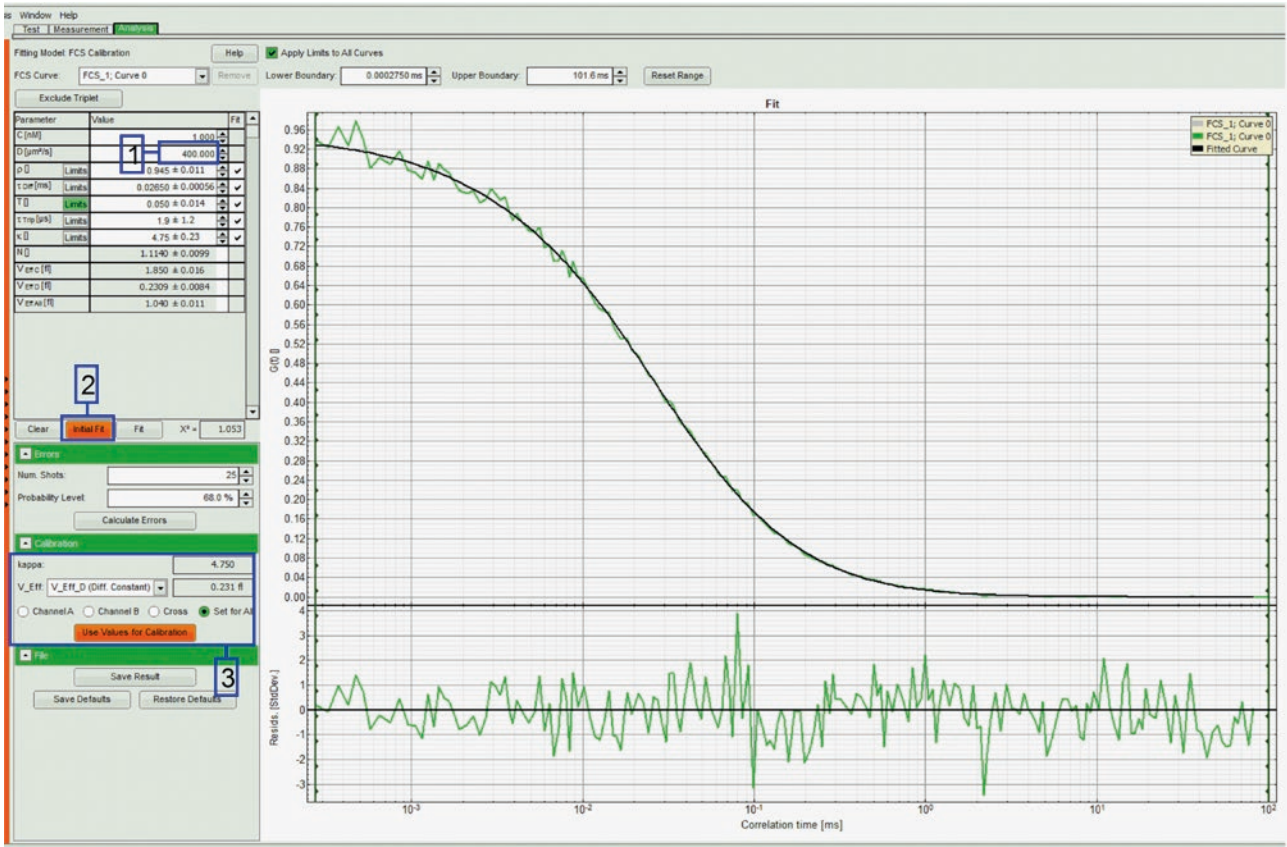


Figure 7

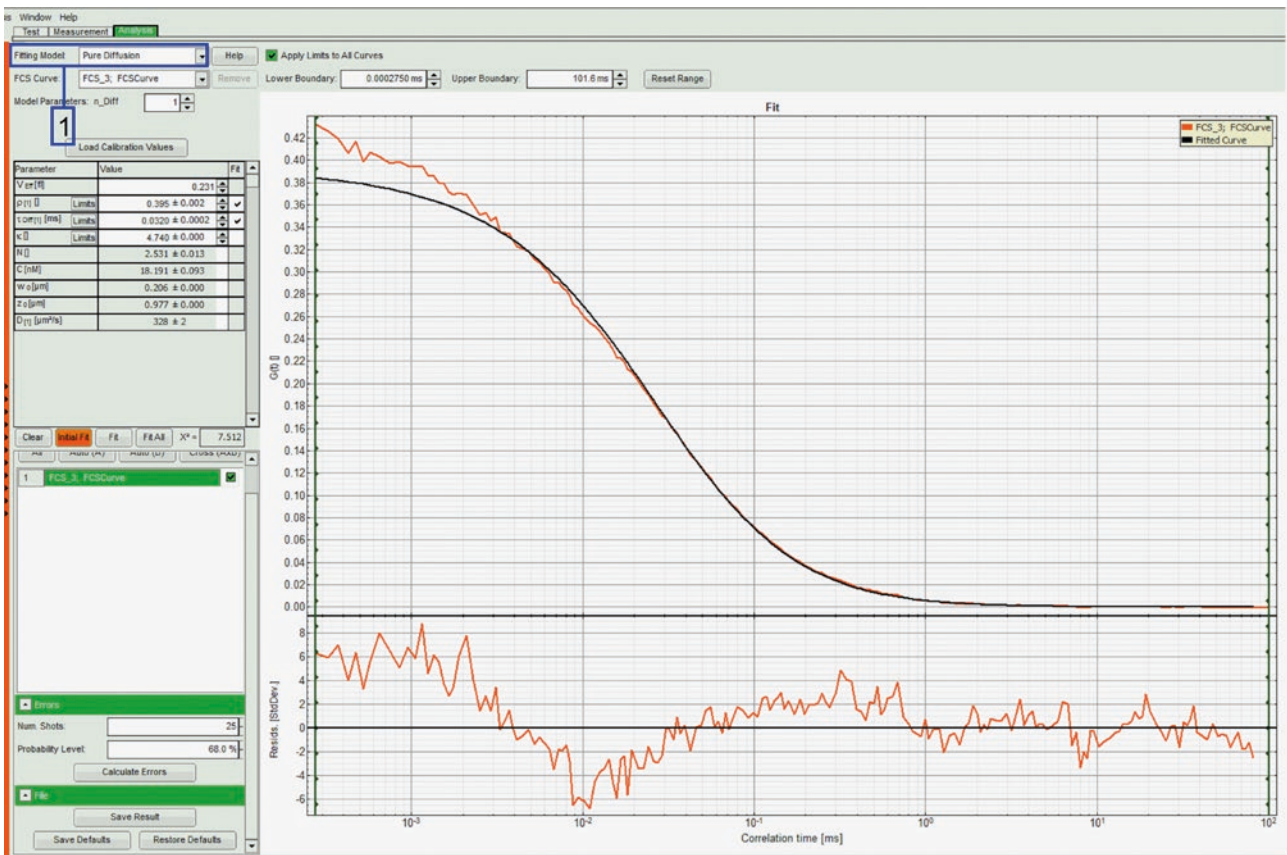


Figure 8

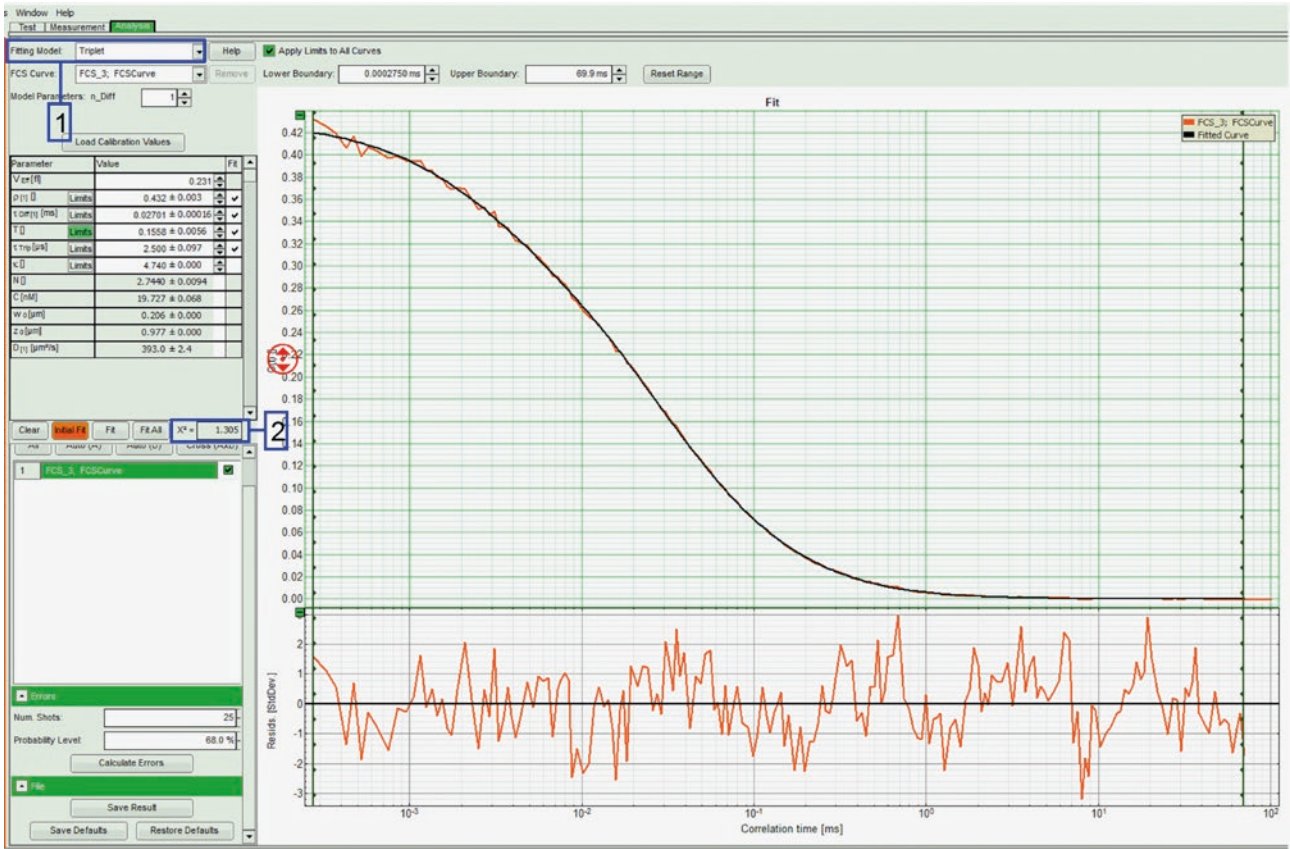


Figure 9

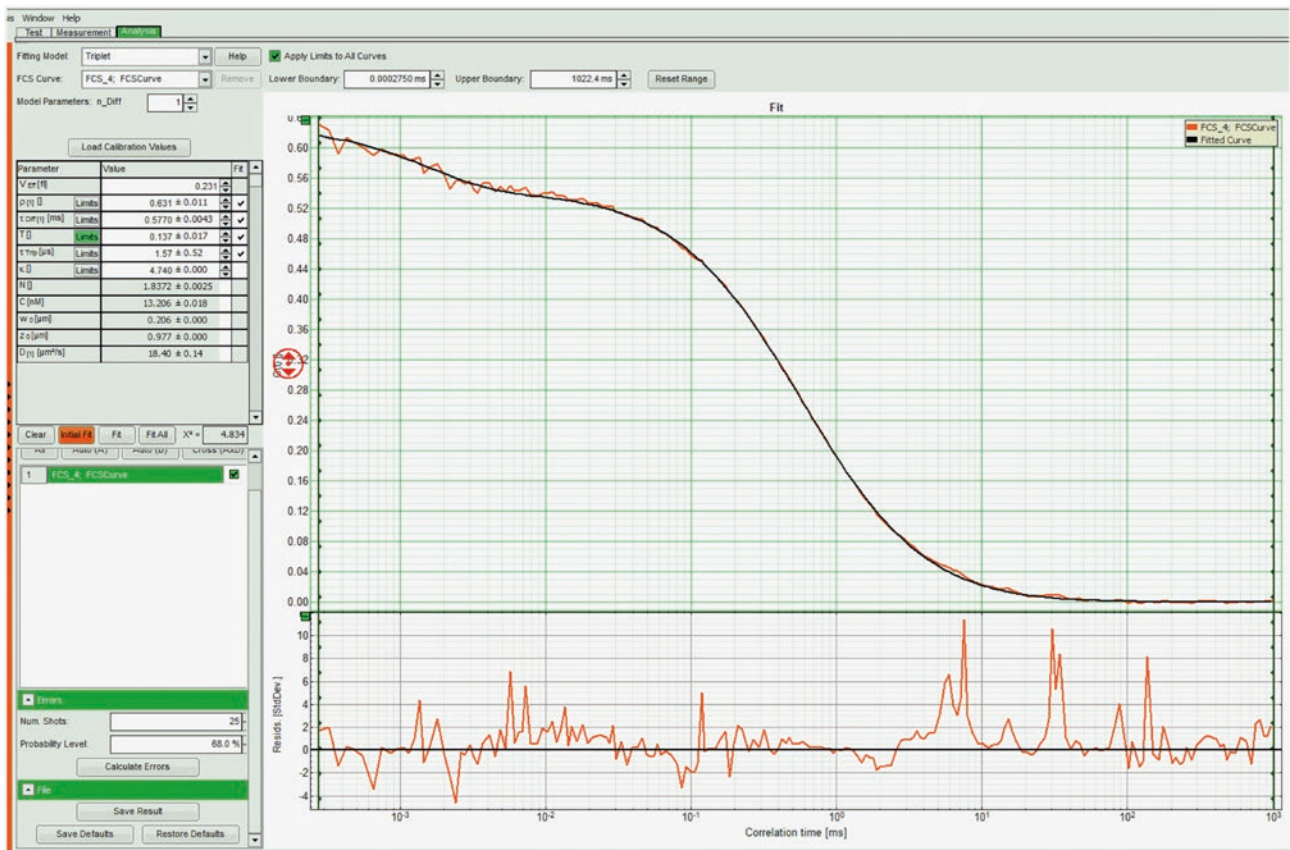


Figure 10

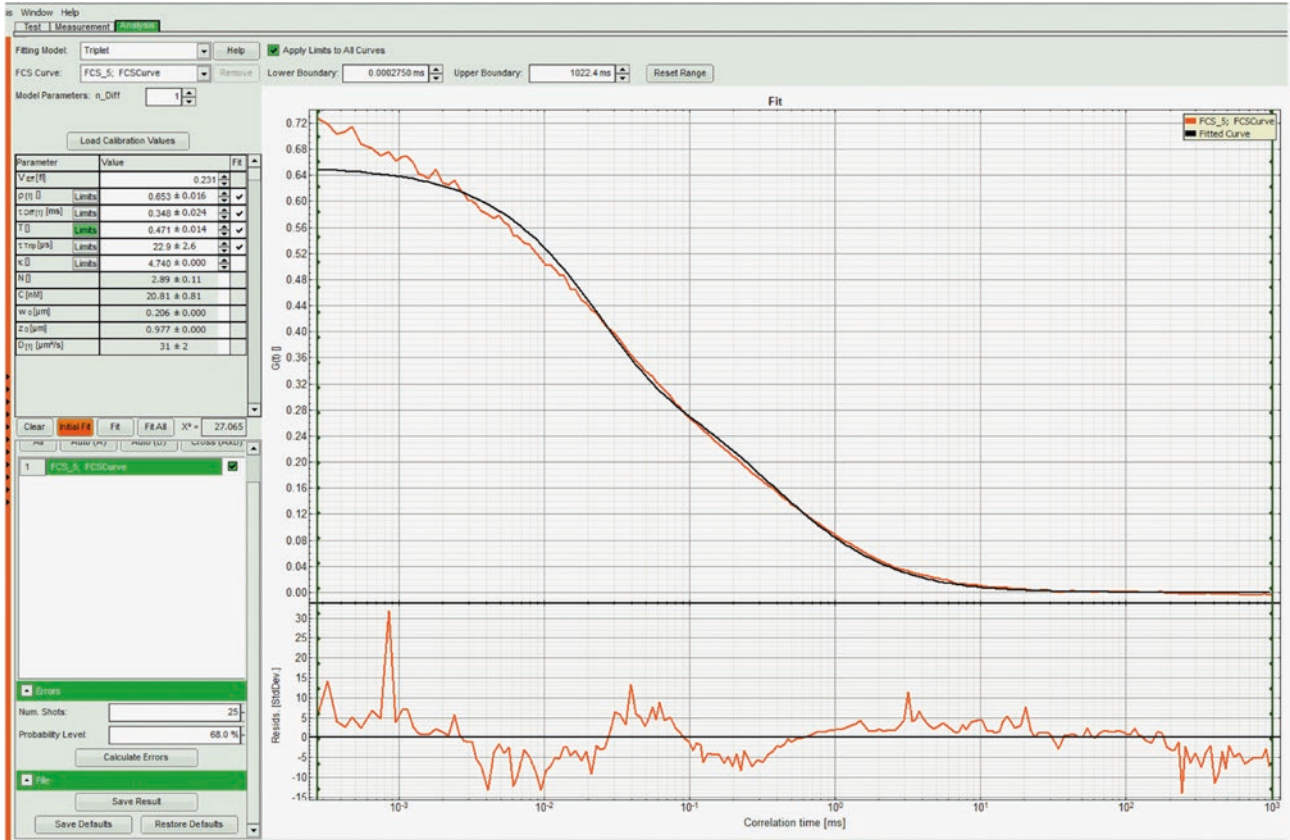


Figure 11

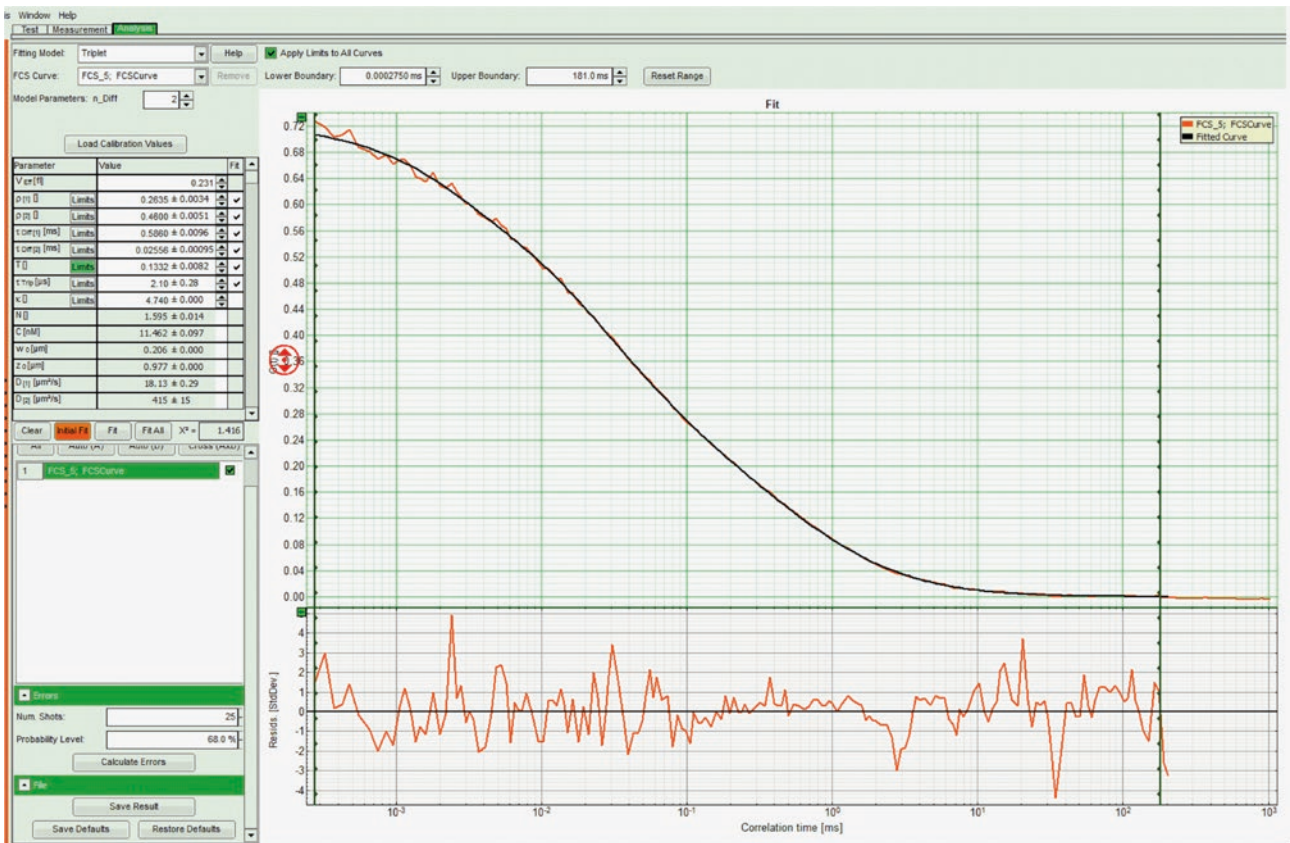


Figure 12